2013-11-27

Determination of the Permeability of the South Chamorro Seamount in Mariana Forearc Crust Using Pressure Response to Tidal Loading Method

Putri N. Akmal
University of Miami, el.akmal@yahoo.com

UNIVERSITY OF MIAMI

DETERMINATION OF THE PERMEABILITY OF THE SOUTH CHAMORRO SEAMOUNT IN MARIANA FOREARC CRUST USING PRESSURE RESPONSE TO TIDAL LOADING METHOD

By

Putri Nur El Akmal

A THESIS

Submitted to the Faculty
of the University of Miami
in partial fulfillment of the requirements for
the degree of Master of Science

Coral Gables, Florida

December 2013

UNIVERSITY OF MIAMI

A thesis submitted in partial fulfillment of
the requirements for the degree of
Master of Science

DETERMINATION OF THE PERMEABILITY OF THE SOUTH CHAMORRO SEAMOUNT IN MARIANA FOREARC CRUST USING PRESSURE RESPONSE TO TIDAL LOADING METHOD

Putri Nur El Akmal

Approved:

_____ Keir Becker, Ph.D. Professor of Marine Geology and Geophysics	_____ Christopher Harrison, Ph.D. Professor of Marine Geology and Geophysics
_____ John Van Leer, Ph.D. Associate Professor of Marine Physics and Oceanography	_____ M. Brian Blake, Ph.D. Dean of the Graduate School

AKMAL, PUTRI N. (Marine Geology & Geophysics)

Determination of the Permeability of the South Chamorro Seamount in Mariana Forearc Crust Using Pressure Response to Tidal Loading Method.

(December 2013)

Abstract of a thesis at the University of Miami.

Thesis supervised by Professor Keir Becker.
No. of pages in text. (63)

ODP borehole observatory 1200C, drilled into the South Chamorro seamount and instrumented with Circulation Obviation Retrofit Kit (CORK), provided information about natural fluid pressure within this forearc crust. The seafloor and formation pressure data recorded hourly and shown fluctuations that are caused largely by the ocean tides. The data also shown two transient pressures increase at the time of two earthquakes. Harmonic analysis provides a simpler way to analyze the periodic tidal signals that constitute the pressure records. By using the result of the harmonic analysis and applying simple theory of formation response to tidal loading, developed by Wang & Davis, the hydrogeologic character of the non-accretionary forearc environment, particularly permeability, can be determined. In this thesis, the way to calculate the permeability of the South Chamorro seamount using CORK-pressure response to tidal loading method and its implication is explained.

The resultant bulk permeability of the seamount is 1.42×10^{-13} m^2, with a range between about 1.18 to 1.79×10^{-13} m^2, that represent the permeability of this formation within the scale of about 176 meter around the CORK-borehole. By using this method we could determine the permeability that represent the formation over the larger scale of investigation relative to other methods,

especially the core-based method as the most common method used to determine permeability. In order to test whether the earthquake would be a factor that would change the permeability of this formation, an analysis is performed, adopting the way that was used in oceanic crust. From the analysis, we could imply that earthquake has negligible effect in changing the formation permeability and it is suggested that this is caused by the elastic behavior of the formation. The matrix frame of this formation, as the component that affect the elastic behavior, is implied to be highly compressible, with its calculated bulk moduli of 0.652 ± 0.15 GPa. The forearc crust has more elastic behavior if compare to the oceanic crust.

ACKNOWLEDGEMENT

As I finished this thesis, I would like to acknowledge many people who have encouraged and helped me throughout this phase of my life. First, I would like to thank my family, especially my beloved parents, Nurhaida Hafni and Mustafa Kemal, and also my sisters, Putri Aqidah and Putri Kemala for always being there for me and giving me all the love and support. They had pushed me to do better and learn more when I'm having this opportunity to continue my study, as this is what I've ever dreamed of when I was in high school. I also want to acknowledge my advisor Keir Becker for giving this opportunity by accepting me into the University. I would also like to thank my thesis committee member: Christopher Harrison and John Van Leer for giving me the constructive feedback on my work. I wouldn't forget to thank the faculty and staff for teaching me and for their kindness and help while I'm studying here in RSMAS.

I would also like to thank my best friends, especially from my undergraduate college, ITB, for being true friends for many years by always keeping in touch and checking my progress and reminding me to be tough throughout this process. I won't forget the kindness and support from my RSMAS friends Keri Vinas, Rani Sianipar, Irena Maura, Qiong Zhang, Caglar Usdun, Deniz Kula, and Deniz Atasoy that made me enjoy my time in Miami. In the end, I also thankful to Allah SWT for his mercy and for all good and bad things I had experienced here in Miami & RSMAS, they were great life lessons for me that will be remembered.

TABLE OF CONTENTS

Page

LIST OF FIGURES

Page

LIST OF TABLES

Page

CHAPTER 1

INTRODUCTION

1.1 Background

Fluid flow in the oceanic crust and through the seafloor occurs in passive continental margins, accretionary and nonaccretionary prisms, mid-ocean ridges, and ridge flanks. It has important effects on the evolution of the lithosphere and on many natural processes, such as deformation processes, subsurface biosphere, and mineral or ore generation. To understand these processes, scientists need to quantify the parameters of this flow. Permeability, which is defined as a measure of the capability of the formation to transmit fluid along a non-hydrostatic pressure gradient (Becker and Davis, 2004), is a property that most directly controls the rates and patterns of the fluid circulation that is important in transferring heat from a cooling lithosphere, in carrying solutes to the seafloor and in altering the composition and physical properties of the crust (Davis et al., 2000). Hence, a good understanding of permeability in the formation of the crust is critical in order to reveal the hydrogeological conditions, as it can be used as one of the constraints for modeling the hydrogeological processes of the crust.

Resolving or constraining the physical and chemical nature of this crustal fluid flow beneath the ocean can be done in part by downhole measurements and sampling. The effort to understand fluid flow within oceanic crust drove scientists to develop long-term subseafloor observatories called Circulation-

Obviation Retrofit Kits (CORKs) (Davis et al., 1992). CORKs generally include pressure gauges, a set of temperature sensors and borehole fluid sampling as downhole instrumentation in boreholes drilled by the Ocean Drilling Program (ODP). The Ocean Drilling Program (ODP) was an international partnership of scientists and research institutions that conduct study into Earth history and structure that are recorded in the ocean basin in order to get a better understanding of plate tectonic processes, Earth's crustal structure and composition, environmental conditions in ancient oceans, and climate change (ODP Final Technical Report, 2007).

Drilling will induce pressure differentials that cause flow between the formation and water column. This flow generates large perturbations that could cause the natural condition of pressures, temperatures and fluid composition to be impossible to determine accurately (Elderfield et al, 2004). CORKs were developed to overcome this problem, by sealing the borehole to let the formation recover back to its equilibrium state. By deploying these instruments, the natural fluid pressure and temperature within the crust could be monitored in-situ and information about thermal, chemical, hydrological, and even biological processes in the crust could be collected.

CORKs have been deployed in various settings where natural fluid fluxes are large, such as in ridge flank and subduction zones. CORKs have been deployed in ODP holes during Legs 139 (Juan de Fuca Ridge), 156 (Barbados accretionary prism), 168 (Juan de Fuca Ridge), 174B (Mid-Atlantic Ridge), and 195 (South Chamorro Seamount) to further understand the fluid budgets

(Salisbury et al., 2002). Studies using CORK data that had been well documented are by far concentrated on the ridge flanks, because they host the greatest proportion of total fluid flow through the seafloor (Elderfield et al., 2004).

In this study, we focus on using the in-situ pressure data from a CORK observatory deployed in a subduction setting, specifically borehole 1200C that was drilled into subseafloor of South Chamorro seamount in Mariana Forearc crust during ODP leg 195. This CORK pressure data will be used to reach the objective of this study, which is to determine and constrain the hydraulic properties, particularly permeability, within this setting. The CORK deployed in this hole was the first to permit study of a non-accretionary subduction environment (Salisbury et al., 2002). Study in oceanic crust (ridge flank) will be used as reference for this study.

1.2. Study Area

1.2.1 Mariana Forearc: South Chamorro Seamount

The Mariana forearc region is located between the trench and the island arc, within the Mariana convergent margin that was formed as a result of the subduction of old (Jurassic ~170 Mya) western Pacific Oceanic plate beneath the Philippine Sea plate. This study area is non-accretionary, i.e. it has an absence of a large prism of accreted sediment. There is only relatively thin (<500 m) volcaniclastic or pelagic sediment cover on the inner trench slope (Oakley, 2007). Non-accretionary forearc convergent margins have been relatively under-studied compared to accretionary margins because the presence of abundant sediment

in accretionary convergent margins has more advantages, for example to study hydrocarbon or ore generation, water-rock (sediment) interaction, engineering and disposal system for hazardous waste. Nevertheless, a non-accretionary convergent margin has advantages in providing the direct access to study the deeper region (i.e. the tip of a downgoing slab and mantle region) that is currently unreacheable by drilling. During the subduction process, some of the raw materials including fluid from the downgoing plate are released into the forearc crust and mantle and then hydrate (serpentinize) the forearc mantle, which flows back to the seafloor through the lithosphere. Thus, the lack of overlying sediments is believed to allow the fluid and material produced at the seafloor to preserve the original signal from the downgoing slab and hydrated mantle. On the other hand, the interaction of the slab fluid with the thick sediment in an accretionary type margin could modify its composition that will make it difficult to study the geochemical & fluid budget in convergent margin (Salisbury et al., 2002).

Knowing the original fluid composition is important to determine the pressure and temperature conditions at the depth of its origin (Salisbury et al, 2002), which could provide some constraints for modeling subduction processes. This slab-derived fluid can be accessed via active serpentinite seamounts. South Chamorro seamount, located about 85 km away from the Mariana trench and under 2930 meters of water depth, is one of the active seamounts in Mariana Forearc region (**Figure 1.1**). This seamount was chosen as a site for study because this seamount is still active, identified by the presence of low

temperature springs and also the presence of mussel beds and other organisms that were being fed by the nutrients coming out from this spring. The summit 200-m-high tumescent knoll of this seamount was drilled for ODP leg 195 and is called Site 1200.

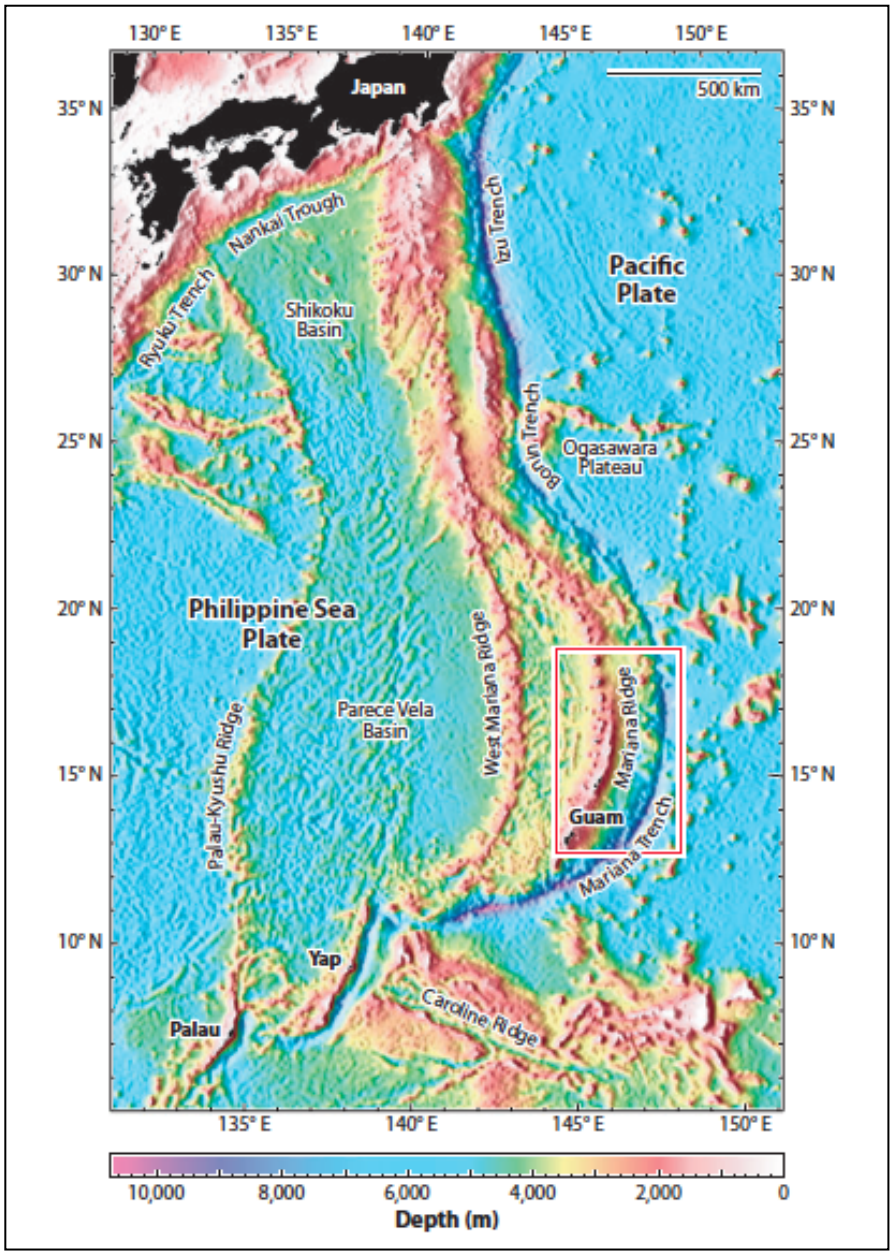

Figure 1.1: Color Bathymetry map showing the study area in a regional context. Red box is the position of figure 1.2. South Chamorro seamount is at 2930 meters of water depth. Figure from Fryer, 2012.

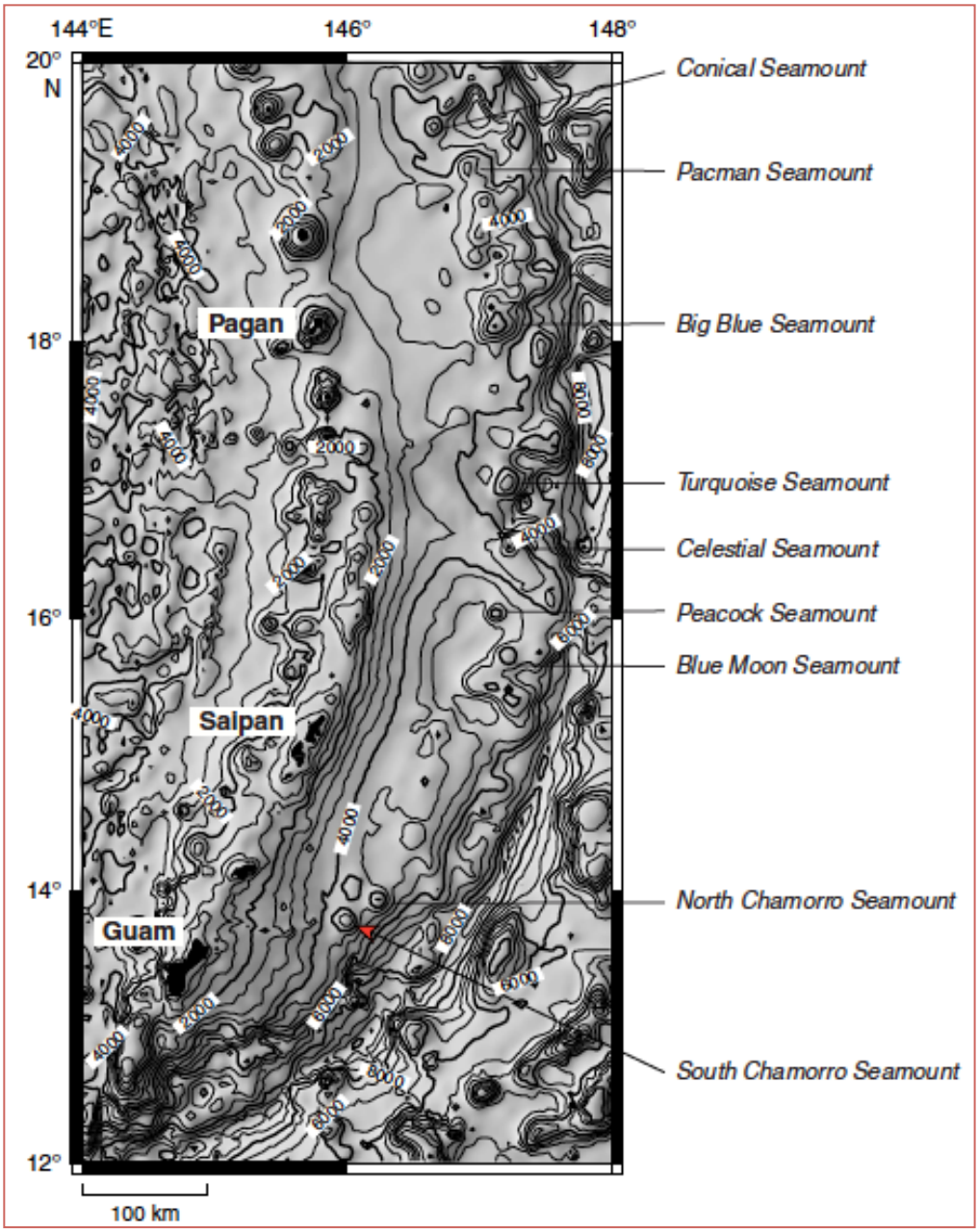

Figure 1.2: Bathymetry of Southern Mariana forearc (500-m contour interval) showing the major seamounts. South Chamorro seamount positioned at 13°47´N, 146°00´E where borehole 1200C is located. Figure from Salisbury et al., 2002.

The seamount represents the output of subduction. It was formed by the serpentinization of the rocks with hydrated slab and mantle material and crustal fluid below the Mariana plate. This created the so-called serpentinite mud that then rose to the seafloor from a central conduit and many faults. A study by

Fryer, 2012 about serpentinite mud volcanism in Mariana forearc summarized that in order for serpentinite mud volcanism to occur, extensional tectonics is required, rather than diapiric mechanisms (as in salt-dome formation). This statement was based on the information that "the serpentine mudflow material is less dense than surrounding peridotite (Ballotti et al. 1992) and should tend to rise because of gravitational instability, but a mixture of serpentinized fault gouge and slab-derived fluids would not be strong enough (e.g., Phipps & Ballotti 1992) to push, diapirically, through surrounding massive peridotite". A conduit for the rise of the serpentinite mud must be created. However, the dynamics of the conduit processes are still unknown. Also, whether seismic activity triggers the eruptive events is still unclear, because some seamounts in the Mariana forearc are associated with clusters of earthquakes, whereas some are not (Fryer 2012). From **Figure 1.3,** South Chamorro seamount is shown not associated with cluster of earthquakes

Based on the analysis of the mud and core samples collected from this Site 1200, South Chamorro seamount is composed mainly of silty clay-sized serpentinite mantle peridotite, and greenschist plus blueschist fragments (Salisbury et al, 2002). Study of pore-fluids in samples from Conical seamount founded that the subducting slab is a source of the serpentinizing fluids and related the change in composition of the fluids with depth to the slab beneath the forearc (Fryer, 2012). From multi-channel seismic data, the downgoing slab lies at around 20 km below the seamount (Oakley, 2007). It was also recognized that chimney structures closer to the trench are composed of brucite, whereas those

farther away are carbonate (Fryer et al. 1999).

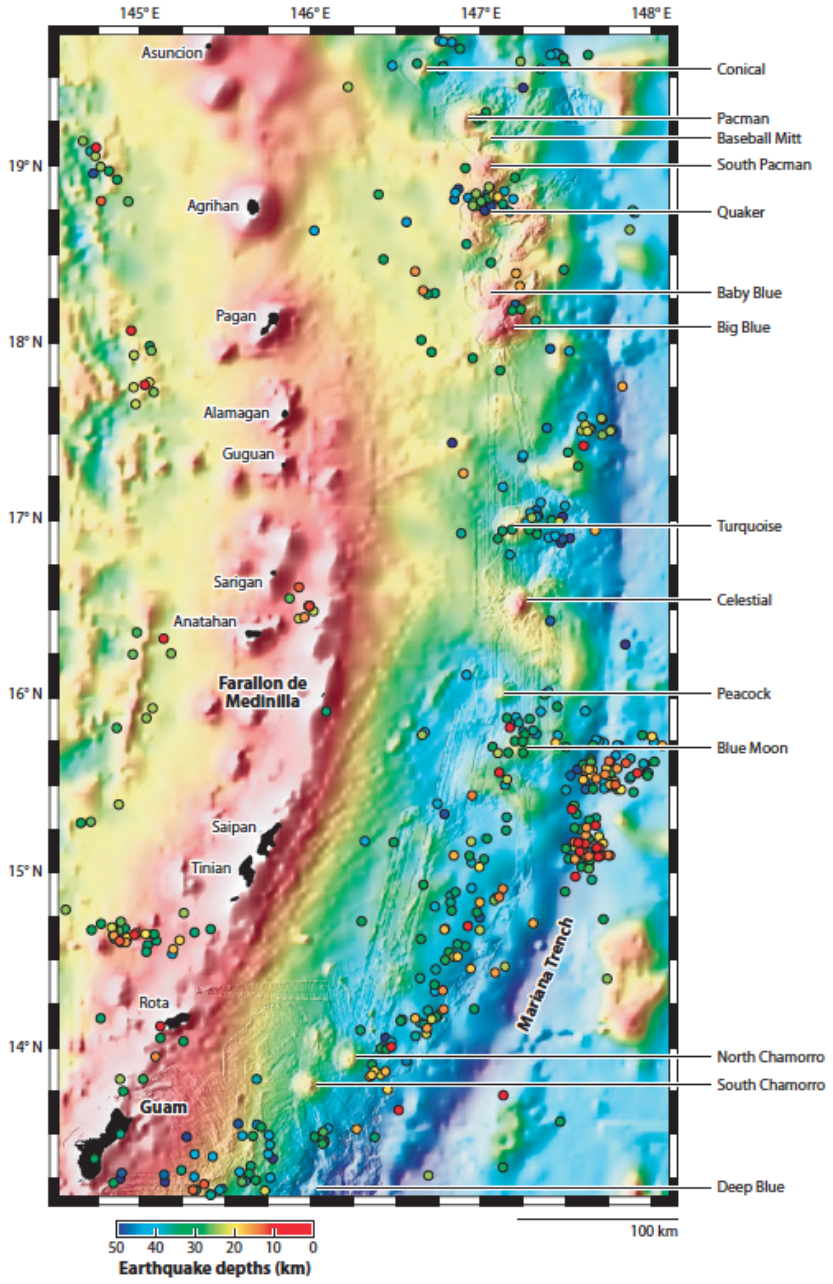

Figure 1.3: Color bathymetry map of Mariana Forearc region showing earthquake locations. Clusters of earthquakes are primarily associated with Blue Moon, Turquoise and Quaker Seamounts. Cluster of events closest to South Chamorro Seamount is found at about 60 km away. Figure from Fryer, 2012.

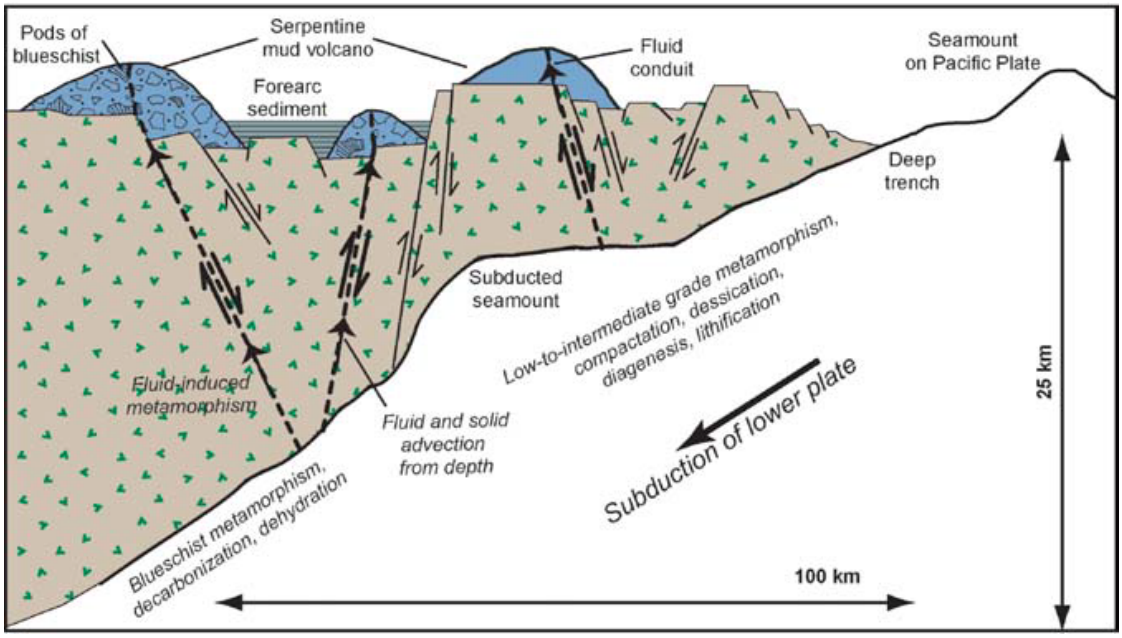

Figure 1.4: Schematic cross section through Mariana subduction system. Strike slip faulting and along strike extension provide pathways for slab-derived fluids to flow. Figure from Fisher, 2005.

1.2.2 Borehole 1200C

Borehole 1200C was drilled on top of South Chamorro seamount at 13°47′N, 146°00′E to a depth of 266 meters below the seafloor (mbsf). This borehole was then instrumented with a Circulation Obviation Retrofit Kit (CORK) that consists of: a casing seal, two pressure transducers, temperature thermistors and two osmotic fluid samplers. This CORK was designed to hydrologically seal a selected section of formation to prevent flow of water into or out of the borehole. During drilling, the formation pressure and temperature condition was perturbed by the injection of cold, dense seawater used as drilling fluid into the warm, less dense formation fluid. CORK sealing allows the formation pressure to recover from the thermal and chemical effects of drilling and approach pre-drilling conditions, so that in-situ hydrological conditions can

be monitored long-term (Davis et al, 1992). Formation fluids could flow into the borehole through the perforated and screened casing section from depth 149 to 202.3 mbsf. The shallower portion of the hole was completely cased, so formation pressures from 149 to 202.3 mbsf were transmitted to the data logger assembly (**Figure 1.6**). Pressures transducers (located inside the data logger assembly) recorded hourly the seafloor and formation pressures starting from the first of CORK deployment on March 25, 2001 until March 17, 2003. Pressure data were downloaded on March 23, 2003, by an ROV (Remote Operating Vehicle). There was no core sample recovered from borehole 1200C during the drilling process. Core samples were collected from nearby boreholes 1200D, 1200E and 1200F that are located at about 40 m, 125 m and 105 m south of hole 1200C, (**Figure 1.5**) and reached depth of 44.4 mbsf, 56.4 mbsf and 16.3 mbsf, respectively (Salisbury et al, 2002).

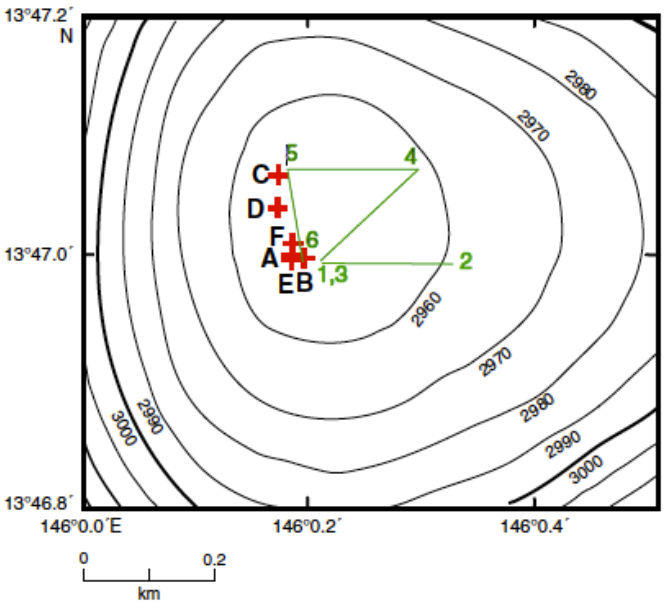

Figure 1.5: Position of Site 1200 holes. Figure from Salisbury et al., 2002

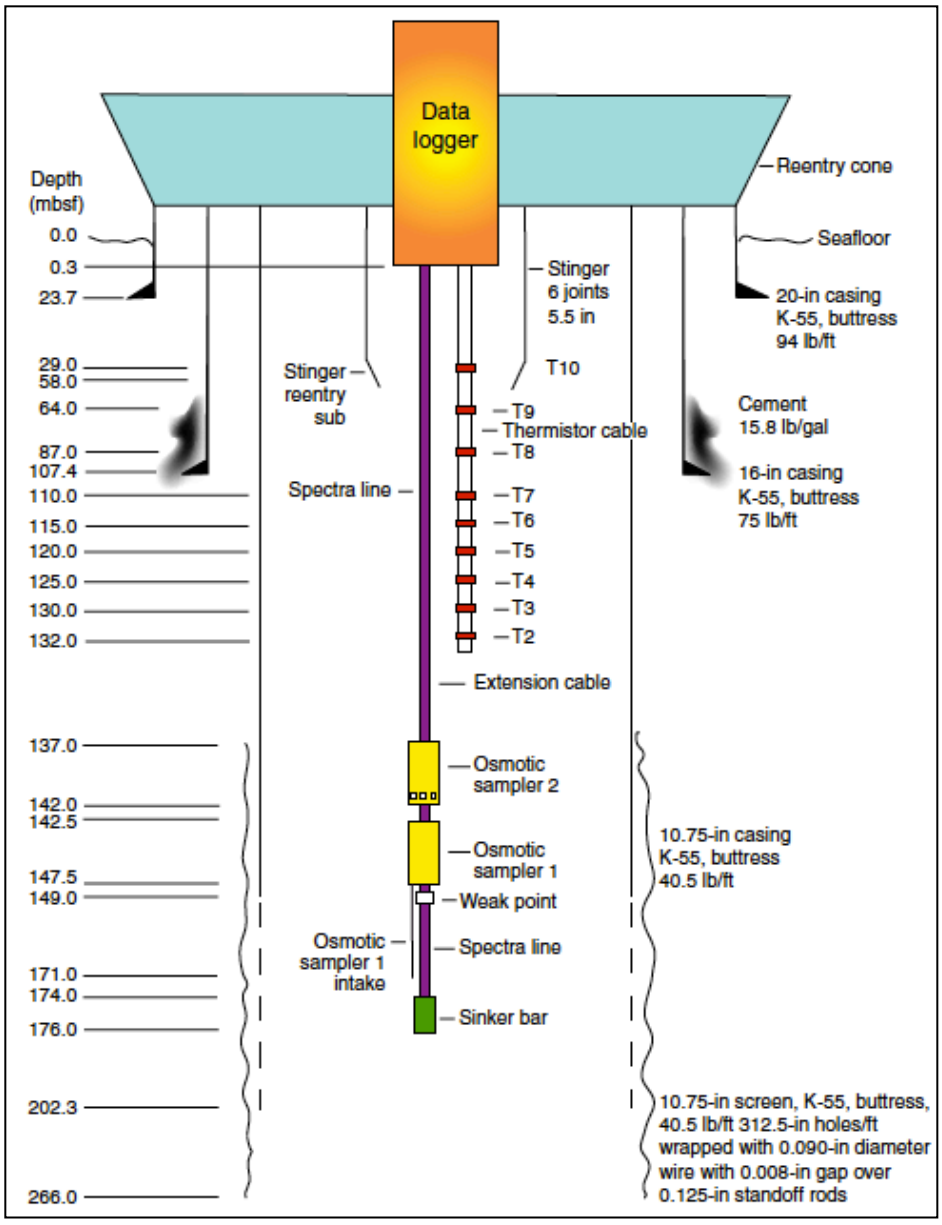

Figure 1.6: Schematic of Circulation Obviation Retrofit Kits (CORKs) deployed in ODP Leg 195 Site 1200C. Figure from Salisbury et al., 2002.

1.3 Datasets

Formation pressure and seafloor pressure records are the primary data for this study. For the initial deployment in 2001, Hole 1200C CORK pressure data logger was set to record pressure every 10 minutes. This was changed to record

the pressure once per hour starting at 15:00 on March 25, 2001. At the beginning, following the CORK installation, the formation pressure shows a gradual build up (rise) as the result of recovery from drilling perturbation and returns to its pre-drilling state. Fluid pressure in the formation and on the seafloor show fluctuations that are caused predominantly by the periodic load of ocean tides on the seafloor and the changes of atmospheric pressure. There are also two transient peaks observed on both formation and seafloor pressure that were recorded at the time of earthquake events (**Figure 1.7)**. The first event was on October 12, 2001 at 15:2:23.3 GMT, which occurred at about 165 km away from 1200C with 7.0 moment magnitude (Mw). The second event on April 26, 2002 at 16:6:13.9 GMT was at 168 km away from 1200C with 7.0 Mw (Data from International Seismological Centre, 2011, Vinas, 2013).

These observed transient responses of formation pressure to external forcing recorded in CORK data could be used in two methods to estimate and constrain permeabilities. They are: 1) The seafloor tidal loading method that uses the effect of seafloor tidal loading on sub-seafloor pressures and 2) The in-situ pressure response to tectonic strain events. These methods had previously been applied in most CORK boreholes in igneous oceanic crust setting. These so-called CORK methods could resolve the permeability over much larger scale of investigation when compared to other methods to estimate permeability as can be seen in **Table 1.1** (Becker and Davis, 2004).

Table 1.1 Approximate lateral scales of investigation for methods used to determine permeabilities of igneous oceanic crust (After Becker and Davis, 2004)

Measurement Method	Approximate scale of investigation (km)
Slug Test	0.001 – 1
Injection Test	0.1 - 10 (test up to 30 minute duration)
Borehole flow thermal methods	1.0 - 10 (depending on duration of flow)
CORK methods and inference from basement isothermality	5.0 - 100 (requires multiple observation points or knowledge of drainage path)

In this study, we will use the naturally occurring fluctuations by ocean tidal loading method in order to determine the formation hydraulic properties. We will only use the hourly-recorded data that are not perturbed by drilling. The transient rise of signals affected by the earthquake also needs to be removed before performing the data analysis. Therefore, before performing the data analysis using this method, the pressure data will be separated into three time series: (1) before the first earthquake event, (2) between the two earthquakes and (3) after the second earthquake (**Figure 1.7)**. The first series started on the record 2700 hours after installation, from June 16, 2001 until an hour before the earthquake (118 days). The time *series 2* started a month after the first earthquake until an hour before the second earthquake (165 days). Time *series 3* had about 234 days from a month after the second earthquake until the last record of pressure data on March 17, 2013.

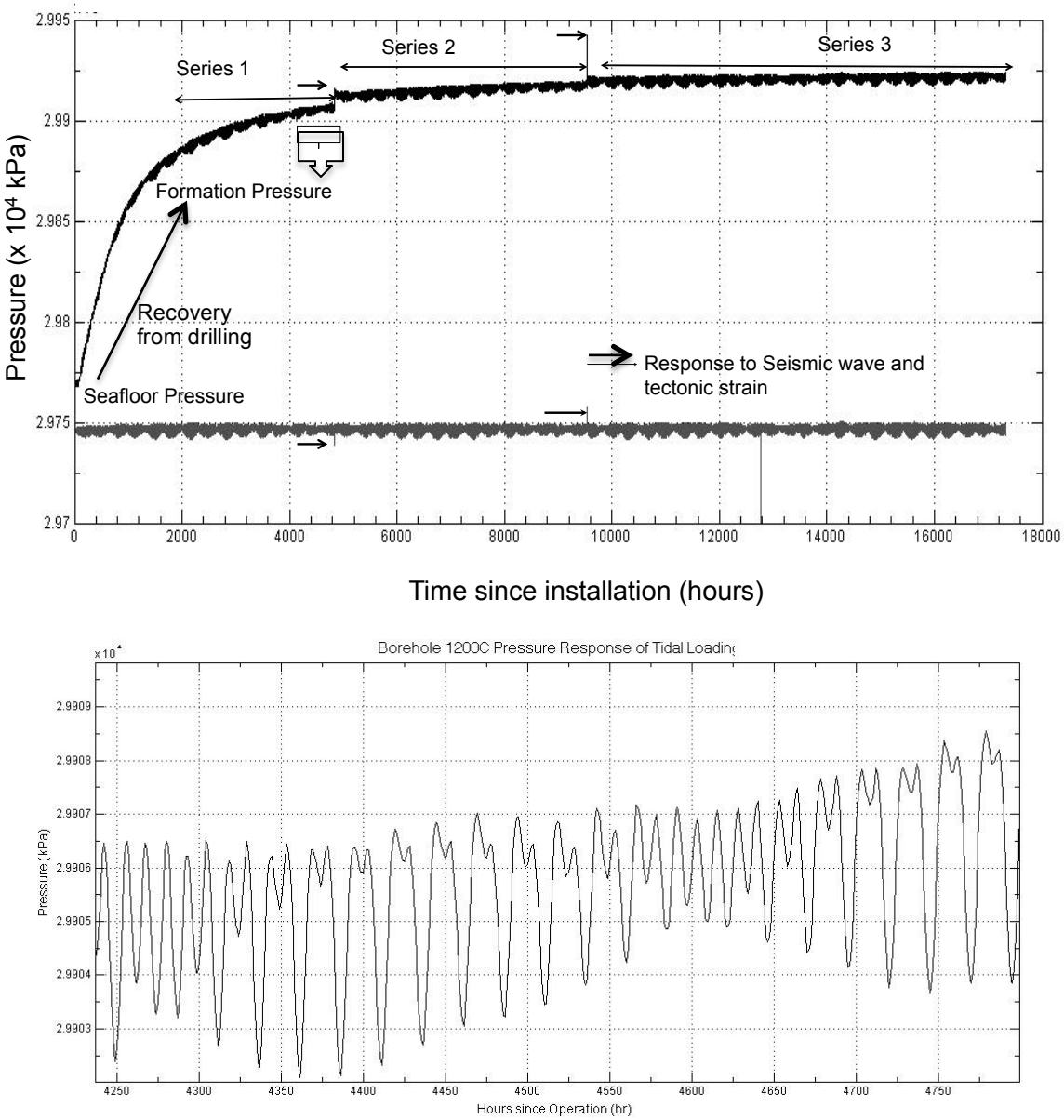

Figure 1.7: Pressure data plot versus time since installation. Fluctuation of seafloor and formation pressure observed (see the enlarged portion) as response to tidal loading. The formation pressures show the recovery of the formation pressures from drilling in the beginning and two pressure transients caused by tectonic strain (Earthquake).

In order to infer and calculate permeability using this tidal loading method, we need to know other formation properties. Poisson's ratio was obtained from measurement of core samples (Courtier et al, 2002). Porosity was taken from

the Wheat et al. (2008) study in Mariana forearc crust. Fluid viscosity, bulk moduli of fluid and bulk moduli of solid constituent of matrix were from reference in oceanic crust sediment by Davis et al. (2000) (**Table 1.2**).

Table 1.2 Formation properties used to determine permeabilities in this study

Formation Properties (Symbol)	Value
Poisson's ratio (v)	0.35 (100% serpentinization)
Porosity (n)	0.45
Fluid viscosity (μ)	0.001 Pa.s
Bulk moduli of fluid (Kf)	2.4×10^9 Pa
Bulk moduli of solid constituent of matrix (Ks)	50×10^9 Pa

1.4. Objectives

Salisbury et al. (2002) stated in the Initial Report of ODP Leg 195 that some of the objectives of drilling at Site 1200 were to:

1) Study geochemical cycling and mass transport in subduction zones and forearc of non-accretionary convergent margins, and

2) Investigate the physical properties of the subduction zone as controls over dehydration reactions and seismicity.

The objective of this study is related to the second objective: specifically to characterize and to constrain the hydraulic properties, particularly permeability of formation in South Chamorro seamount. For this study, we will use the SI unit for permeability, i.e. the square meter (m^2), although the c.g.s. unit, Darcy (D) and milidarcy (mD), are also widely used in petroleum engineering and geology. One Darcy is equivalent to 9.869233×10^{-13} m^2.

1.5 Working Hypotheses

In order to focus the objectives of this research, we test two hypotheses:

1) The estimated value of permeability using pressure data from in-situ measurement will be greater than core-based measurements and more representative of large-scale formation permeability.

As previously mentioned, the seafloor and formation pressure measured in-situ in CORK boreholes can be used to estimate the permeabilities and resolve much larger scale of investigation in an ocean crustal setting. Measurements using core samples might be the simplest way to estimate the permeability. However, core measurements do not resolve the scale dependence, because of the heterogeneity of formation parameters (Becker and Davis, 2004) and also because fractures may not be sampled in the recovered core, especially from formation with lots of fractured rock. Analysis of in-situ pressure data using the tidal loading method may allow us to estimate permeability that would represent formation scale and would yield greater permeability, as suggested from analysis of CORK data in oceanic crust.

To test this hypothesis in forearc crustal areas, we will use the naturally occurring fluctuations in CORK pressure data that are caused by ocean tidal loading (tidal loading method) to resolve the permeability and then we compare this permeability with permeabilities measured in a previous study within this Mariana Forearc region using other methods. The previous study by Wheat et al. in 2008 included permeability determinations by: (1)

laboratory measurement method of core samples from other active mud volcanoes in Mariana forearc crust (Pacman seamount) and (2) the borehole flow method with radial diffusion equation, constrained by flow rate of fluid from the formation and fluid overpressure measured in-situ in South Chamorro seamount. Permeabilities measured at Pacman Seamount range from 10^{-17} m^2 to 10^{-13} m^2 (10^{-15} to 10^{-17} m^2 for blue mud samples and 10-^{13} to 10^{-15} m^2 for volcanic sample). Permeability measured using borehole flow method at Hole 1200C was calculated to be 6 x$10^{-14}$$m^2$.

2) Tectonic activity would change and possibly lead to enhancement of the formation permeability.

Hydrogeologic observation in oceanic crust has shown changes in amplitude and phase of the loading response at the time of large strain events. Amplitude and phase of the loading response represents the elastic and hydraulic properties, therefore the observed changes suggest that the properties in oceanic crust are sensitive to strain during earthquakes. These changes are then slowly returned to former values (before the earthquake) over a period of many months (Davis and Becker, 2004). We would like to test this hypothesis in a forearc setting as there are two transient peaks, that were observed in CORKs pressure data for this study and were recorded at the time of earthquake event. We will adopt the method used in oceanic crust to observe the changes in amplitude and phase of the loading response. In addition, the data conditioning, i.e. separating the data into three time series, would also allow us to test this hypothesis.

CHAPTER 2

METHODOLOGY

This study uses CORK pressure data in order to determine the hydrological properties of the South Chamorro seamount. The pressure fluctuations in response to ocean tidal loading observed in the data were analyzed using Tidal Analysis Program in Python (*TAPPy*) and the results were further analyzed by matching it with the theoretical model developed by Wang and Davis (1996) in order to determine the formation properties.

2.1 Pressure Response to Tidal Loading

The fluctuation of pressure observed in the data is a response to the periodic tidal loading on the seafloor that created periodic changes in overburden pressure and thus affects the formation pressure. The stresses caused by tidal load create strains in the formation that will give changes in pressure. Pressure signals are generated at any boundary where there is a contrast in the elastic properties. At relatively low frequencies, these signals will transfer throughout the elastic medium (formation) with amplitude and phase varies with depth or length of its propagation that depend on formation properties (Davis et al., 2000; Wang and Davis 1996; Van der Kamp and Gale 1983). Therefore, we can use this fluctuation of fluid pressure to deduce formation properties.

The pressure fluctuations induced by tidal loads had been discussed and many authors had developed models that illustrate their relationship with

formation properties. Biot introduced the initial model around the 1940s to describe wave propagation in a poroelastic medium. It was adopted by Van der Kamp and Gale (1983) to develop a model describing the tidal loading effects in fluid pressure response, which in general could be applied in geophysics, geomechanics and engineering field. Wang and Davis (1996) have developed a model for application in hydrogeology in oceanic crust for ODP boreholes. They presented the pore pressure variation models for the simple case of a one-layer media or so-called uniform half-space and for layered media. For this study, we will use the simple uniform half-space model as we consider the lithology of the formation is dominated by serpentinite mud and almost uniform (according to lithostratigraphic study from core sample in Salisbury et al, 2002; **Appendix**), with the primary boundary for the system at the seafloor. For the application in CORK ODP borehole in oceanic crust, this model has been discussed in paper by Davis et al, 2000 and book by Davis and Becker, 2004 and is summarized here to illustrate the method used for the calculation of formation properties in this study.

The formation pressure signals generated by a combination of elastic and diffusive response to time-varying tidal load:

Elastic response

The rock is considered as a medium consists of solid matrix and pore fluid that would deform elastically when there is load applied **(Figure 2.1).** When the medium is compressed by the tidal load, the load is shared between the matrix frame and pore fluid. The fraction of load taken up by the fluid is called the

loading efficiency (**γ**). When the matrix is less compressible, it will take up more of the load and therefore the fluid takes less of the loads making the loading efficiency small. Conversely, the more compressible the matrix, the fluids will take the greater share of the load, thus the larger the loading efficiency. The load taken by the fluid is the component that contributes to give changes in fluid pressure (formation pressure). Consequently, elastic response depends on the elastic properties. Porosity also contributes to the fluid pressure, where higher porosity will enhance the effect of fluid compressibility (Becker and Davis, 2004). The elastic property is commonly called elastic modulus, which is the inverse of compressibility and is a measure of overall rock stiffness. For the rock system, it consists of three components; bulk moduli of the fluid, bulk moduli of the matrix frame and bulk moduli of the solid constituent of the matrix.

The relation between loading efficiency and elastic properties is simplified by Jacobs (1940), assuming the solid constituents are incompressible (Davis et al, 2001). This simple relation will be used for this study:

$$\gamma = \frac{1}{1 + n(\frac{K'}{Kf})} \quad \text{.....(1)}$$

and

$$K' = 3K\frac{(1-v)}{(1+v)} \quad \text{.....(2)}$$

where

K =frame bulk modulus (Pa)

K’ = 1-Dimensional frame bulk modulus (Pa)

n = porosity,

γ = loading efficiency,

Kf = bulk modulus of fluid (Pa)

v = Poisson's ratio (of frame?).

The one-dimensional frame bulk modulus means no horizontal deformation of the frame bulk modulus (the compaction is only in the vertical direction and that the strain in the horizontal direction is zero).

Diffusive response

At low loading frequency, the difference in loading efficiency causes change in fluid pressure, and therefore created pressure gradient across the interface, that will allow fluid to flow and propagate the signal. This pressure gradient that propagates the signal is called diffusive part of the pressure response. The diffusion that occurs is governed by the hydraulic diffusivity (**η**). Hydraulic diffusivity is a parameter that combines transmission characteristic (permeability) and storage properties (effective compressibility).

$$\eta = \frac{\kappa}{\mu S} \quad \text{.....(3)}$$

where:

k = permeability (m^2)

μ = fluid viscosity (Pa s)

S = effective compressibility (Pa^{-1})

$$S = \left(\frac{1}{K} - \frac{1}{Ks}\right)\left(1 - \frac{2\alpha(1-2v)}{3(1-v)}\right) + n\left(\frac{1}{Kf} - \frac{1}{Ks}\right) \quad \text{.....(4)}$$

where

K =frame bulk modulus (Pa)

Ks= bulk modulus of solid constituent of matrix (Pa)

Kf = bulk modulus of fluid (Pa)

α = elasticity parameter = 1 – Kf/Ks …….....(5)

v = Poisson's ratio

n = porosity

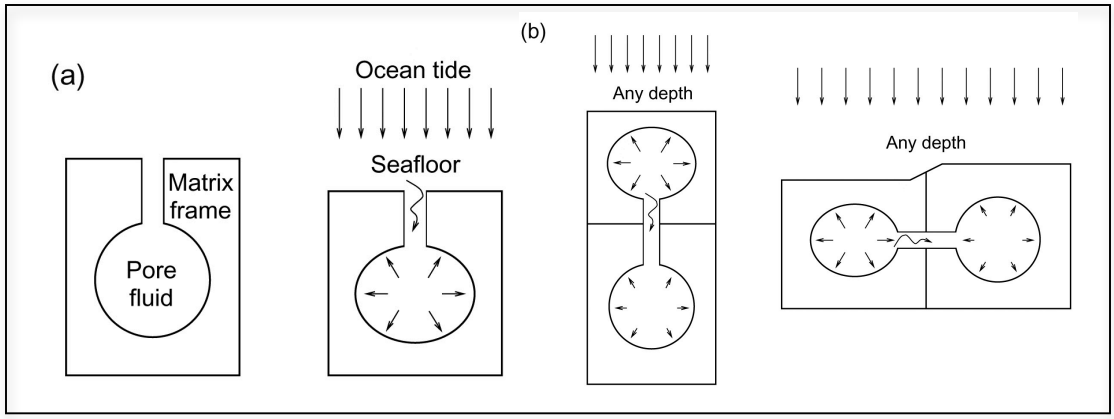

Figure 2.1: Cartoon illustrating a) medium consisting of a solid matrix frame and pore fluid & it's elastic response to ocean tide load on the seafloor b) diffusive response: fluid flow (vertical & horizontal direction) caused by the differential fluid pressures created by the contrast in loading efficiencies. Figure from Becker and Davis (2004).

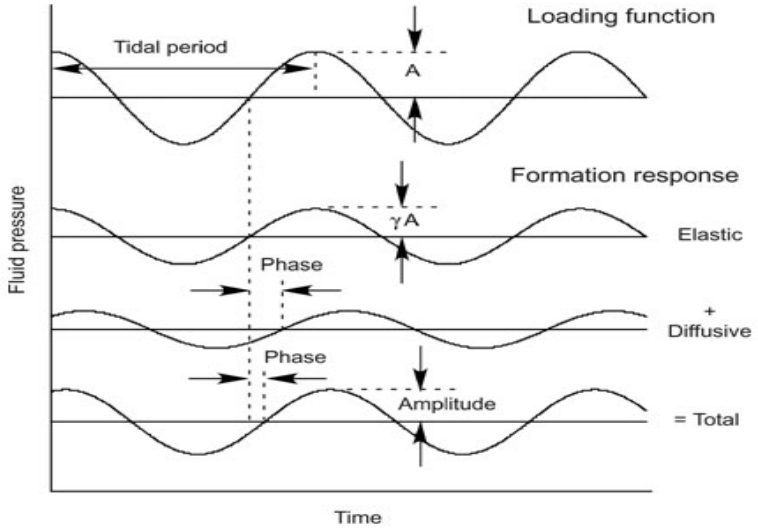

Figure 2.2: Illustration of the formation responses to tidal loading. The loading function is the time-varying load in seafloor. Pressure signal attenuates (elastic response) and the phase of the signal is shifted (diffusive response). From Becker and Davis (2004).

Loading efficiency affects the magnitude of the signal's attenuation as it propagates from the seafloor to the formation and the diffusion occurring within the formation, depending on the distance from this interface, may cause a phase lead or lag of the formation pressure response. When the elastic and diffusive response is combined it shows the signal propagation with amplitude that decreases with depth and phase lead or lag that varies with depth (see **Figure 2.2**).

The solution from Wang (2004) that illustrates the total formation response is as follows:

$$P\,(z,t) = \sigma_b \left[\underbrace{\gamma' \cos\left(\frac{2\pi t}{T}\right)}_{\text{Elastic component}} + \underbrace{(1-\gamma')e^{-\frac{\pi z}{d}}\cos\left(\frac{2\pi t}{T}-\frac{\pi z}{d}\right)}_{\text{Diffusive component}}\right]$$

d, the penetration depth of diffusive pressure signal, is equal to the half wavelength of this signal that depends on hydraulic diffusivity and period.

$$d = \sqrt{(\pi\ \eta\ T)} \quad \text{.....(6)}$$

where:

d = penetration depth or propagation length (m)

η = hydraulic diffusivity ($m^2\ s^{-1}$)

T = period (sec)

and dimensionless depth

$$\zeta = \frac{d}{\sqrt{\pi\eta T}} \quad \text{..... (7)}$$

Dimensionless depth of 1 is equal to the half wavelength of the pressure signal of

period T.

Based on the solution, Wang and Davis plotted the amplitude ratio and the phase difference as functions of the dimensionless depth (**Figure 2.3** & **Figure 2.4**). At the penetration depth and deeper, the pore pressure change is almost entirely elastic response, meaning no net fluid flow. At this depth, the amplitude of formation pressure signal is constant with the amount of attenuation and is equal to the loading efficiency of the formation. Hence, the amplitude ratio versus dimensionless depth plot can be used to deduce loading efficiency. Also, at this penetration depth, the formation pressure signal is in phase with the seafloor signal. Therefore, the zero-phase crossing in the plot of phase lag versus dimensionless depth can be used to deduce this penetration depth (d). When combined with other formation properties (equations 1 to 4), these deduced parameters, loading efficiency and the penetration depth, allow us to estimate the framework bulk modulus and permeability, respectively.

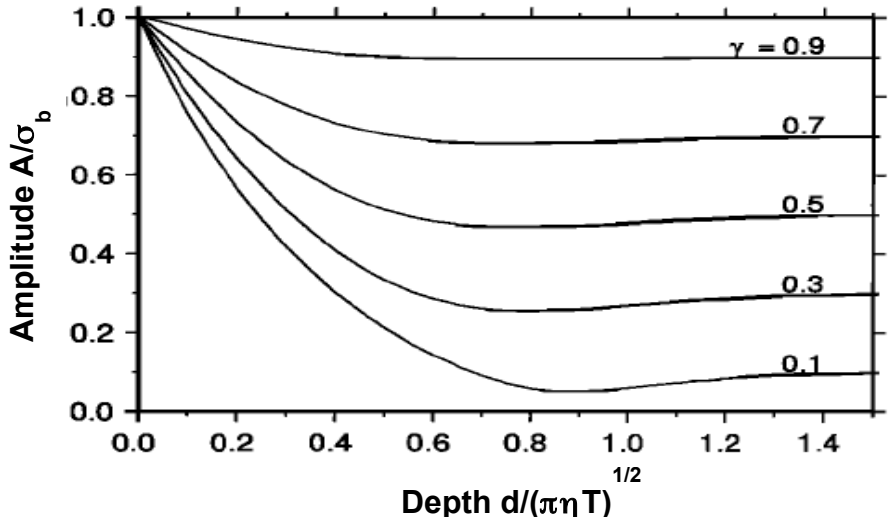

Figure 2.3 Plot of Amplitude ratio versus dimensionless depth (Modified from Wang & Davis, 1996)

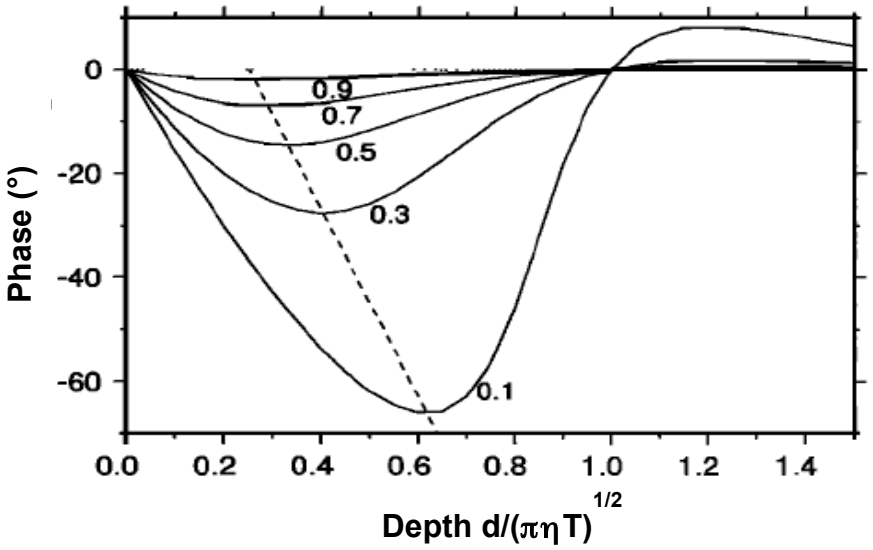

Figure 2.4 Plot of Phase difference versus dimensionless depth (Modified from Wang & Davis, 1996)

2.2 Harmonic Analysis

In order to calculate the amplitude and phases for both seafloor pressure and formation pressure, we need to perform harmonic analysis. This analysis decomposes an hourly time-series of pressures into the tidal components, i.e. amplitude and phases of a set of sine waves. One set of sine waves represents waves for one tidal constituent (tidal wave with typical period or frequency). This analysis was performed using Tidal Analysis Program in Python programming software (*TAPPy*) which uses the least squares optimization and other function available in this Python programming software (*SciPy*). As described earlier the pressure data are separated into three series of time: (1) before the first earthquake event, (2) after the first earthquake and (3) after the second earthquake. Harmonic analysis was performed for each series of each type of pressure data. To run the tidal analysis program in Python, these data containing time and pressure built in text format (.txt) and required an additional file called

'data definition', also in text format, used to define the variables inside the main data. One advantage using this program is that we can eliminate if any linear trend, i.e. the sinusoid generated from the long records of pressure does not resemble a tidal cycle, exist in the pressure data only by adding specific code in the command line to run the program. If needed, the tidal effect can be removed with tide elimination filter to get the clean pressure data (de-tide the pressure data). The output contains the tidal components measured for each tidal frequency resolved in the pressure time-series data. The example of data definition file and the result is enclosed in **Appendix.**

2.3 Earthquake Effect in Formation Properties

In order to see if there was any change in the permeability caused by the earthquake, we shall observe if there is any change in both phase and amplitude of the formation response at and after the times of earthquake. We could see the changes between the three time series or for more detail analysis we can break the data into 29 days intervals, this way we will obtain the similar tidal constituents for each interval, and the possibility to include the monthly tidal constituent. This method is adapted from the one used for pressure data from ODP borehole drilled in oceanic crust of the Juan de Fuca area (Davis and Becker, 2004). In this area, they observed changes in phase and amplitude response of the strongest tidal constituent (M2) at the times of the three seismogenic slip events in the region; NTF (Nootka Transform Fault), JFR (Juan

de Fuca Ridge) and JFP (Juan de Fuca Plate). This example is shown in **Figure 2.5**

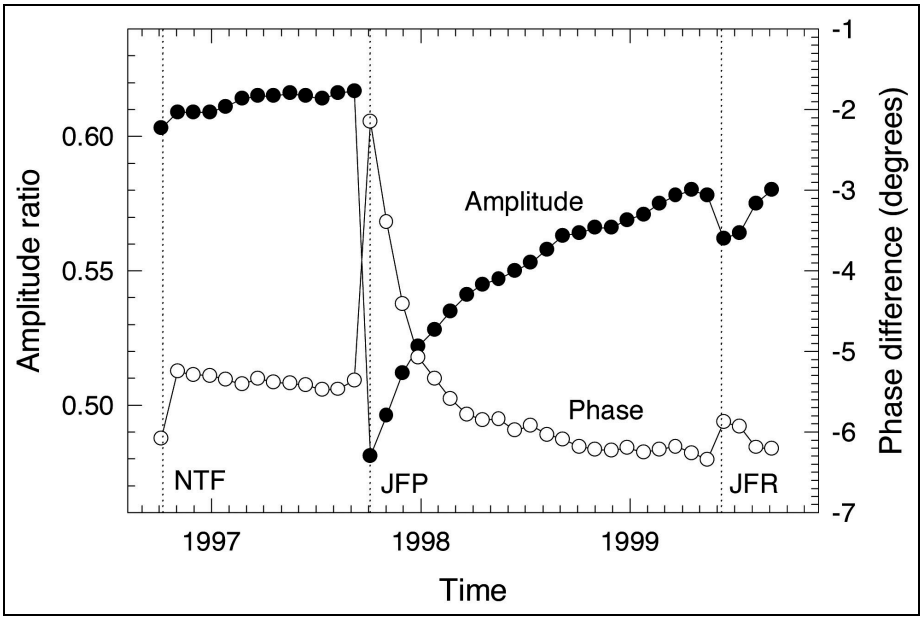

Figure 2.5: Phase and amplitude of formation tidal signals relative to seafloor loading, calculated for 28-day windows over a 3-year observation interval at ODP Hole 1025C, Juan de Fuca Ridge flank. Response at the strongest M2 tidal constituent is shown; Changes in both phase and amplitude of the formation response are seen at the times of three seismogenic slip events in the region. Similar behavior is resolved at other dominant frequencies (e.g., K1, O1). Figure from Davis & Becker (2004).

CHAPTER 3

ANALYSIS OF HYDROGEOLOGIC PROPERTIES OF SOUTH CHAMORRO SEAMOUNT

3.1 Overview

In this study, we considered flow of a single-phase fluid (liquid) through South Chamorro Seamount assuming it is a single layer, homogeneous and isotropic formation and that the propagation pathway for the diffusion wave is directly from the boundary (seafloor) until the average depth of open/screened borehole (the average between 149 to 202 mbsf, which is ±176 m). Therefore the scale of investigation for permeability measurement in this formation is ±176 m both vertically and laterally from the borehole.

Tides, which are forced oscillation resulting from celestial motion, occur at known frequencies and create tidal signals or sinusoidal waves with constant amplitude and phase that is called tidal constituents. Many tidal constituents may exist that depend on the hydrodynamics of the region (Boon, 2004). The length of time of the record also determines the number of tidal constituents that could be resolved using the harmonic analysis. Harmonic analysis will reveal the amplitude and phase of these tidal constituents. The results of harmonic analysis of each time series for both seafloor and formation pressure using TAPPy can be seen in **Appendix.**

For further analysis using simple theory by Wang & Davis (1996), we only use the tidal constituents of both seafloor pressure and formation pressure that have amplitude bigger than 0.1 kPa (H>0.1 kPa in **Appendix).** Those tidal constituents are summarized in **Table 3.1.** They are dominated by diurnal and

semidiurnal band. The five major constituents that usually exist are O1 (*lunar diurnal*, period = 25.82 hours), K1 (*luni-solar diurnal*, period = 23.93 hours), N2 (*larger lunar elliptic semidiurnal*, period = 12.66 hours), M2 (*principal lunar semidiurnal*, period = 12.42 hours), S2 (*principal solar semidiurnal*, period = 25.82 hours). The amplitude ratio and phase difference for each tidal constituent and for each time series is summarized in **Table 3.1** and are used for the analysis of hydraulic properties.

In addition, the Fourier periodogram or power spectrum can often identify important tidal constituents from energy peaks associated with specific frequencies (Boon, 2007). Power spectra of the constituents for the seafloor and each series of formation records resulted from spectral analysis using MATLAB are shown in **Figure 3.1** suggesting K1 as the strongest tidal constituent in this area and followed by O1 and M2 constituents that were also resolved clearly in each periodogram. From spectral and harmonic analysis, we could see the propagation of pressure signal following the theory of tidal signal propagation; the signals were attenuated, which means the amplitude of the signals getting decrease and the phase of the signals change as it diffuses from the seafloor into the formation.

Table 3.1: Characteristic of Primary Tidal Constituents of Formation Pressure Variations relative to Seafloor Pressure (Tidal function) resulted from Harmonic Analysis for Each Time Series

No	TIDAL HARMONIC CONSTITUENT	Symbol	PERIOD (solar hours)	Distance / √Period (m / sec^½)	AMPLITUDE RATIO (Formation/Seafloor amplitude)			PHASE DIFFERENCE (Formation-Seafloor Phase)		
					SERIES 1	SERIES 2	SERIES 3	SERIES 1	SERIES 2	SERIES 3
1	Lunisolar fortnightly	Mf	327.86	0.162			0.921			0.2861
2	Larger lunar elliptic diurnal	Q1	26.87	0.566	0.867	0.835	0.838	-0.5112	-0.3294	-0.3018
3	Lunar diurnal	O1	25.82	0.577	0.831	0.835	0.828	-0.5259	-1.0149	-0.9164
4	Smaller lunar elliptic diurnal	M1	24.84	0.589			0.828			-3.1585
5	Solar diurnal	P1	24.07	0.598	0.841	0.834	0.839	-0.0128	-0.0124	-0.4017
6	Luni-solar diurnal	K1	23.93	0.600	0.841	0.834	0.834	-0.7498	-0.6846	-1.0163
7	Smaller lunar elliptic diurnal	J1	23.10	0.610		0.845	0.853		-0.331	-1.5307
8	Lunar diurnal (second order)	OO1	22.31	0.621			0.846			-1.3091
9	Larger lunar elliptic semidiurnal	N2	12.66	0.824		0.844	0.877		0.645	1.4628
10	Principal lunar semidiurnal	M2	12.42	0.832	0.872	0.872	0.867	-0.3153	0.5812	1.9889
11	Principal solar semidiurnal	S2	12.00	0.847	0.829	0.876	0.831	0.366	2.567	5.5615

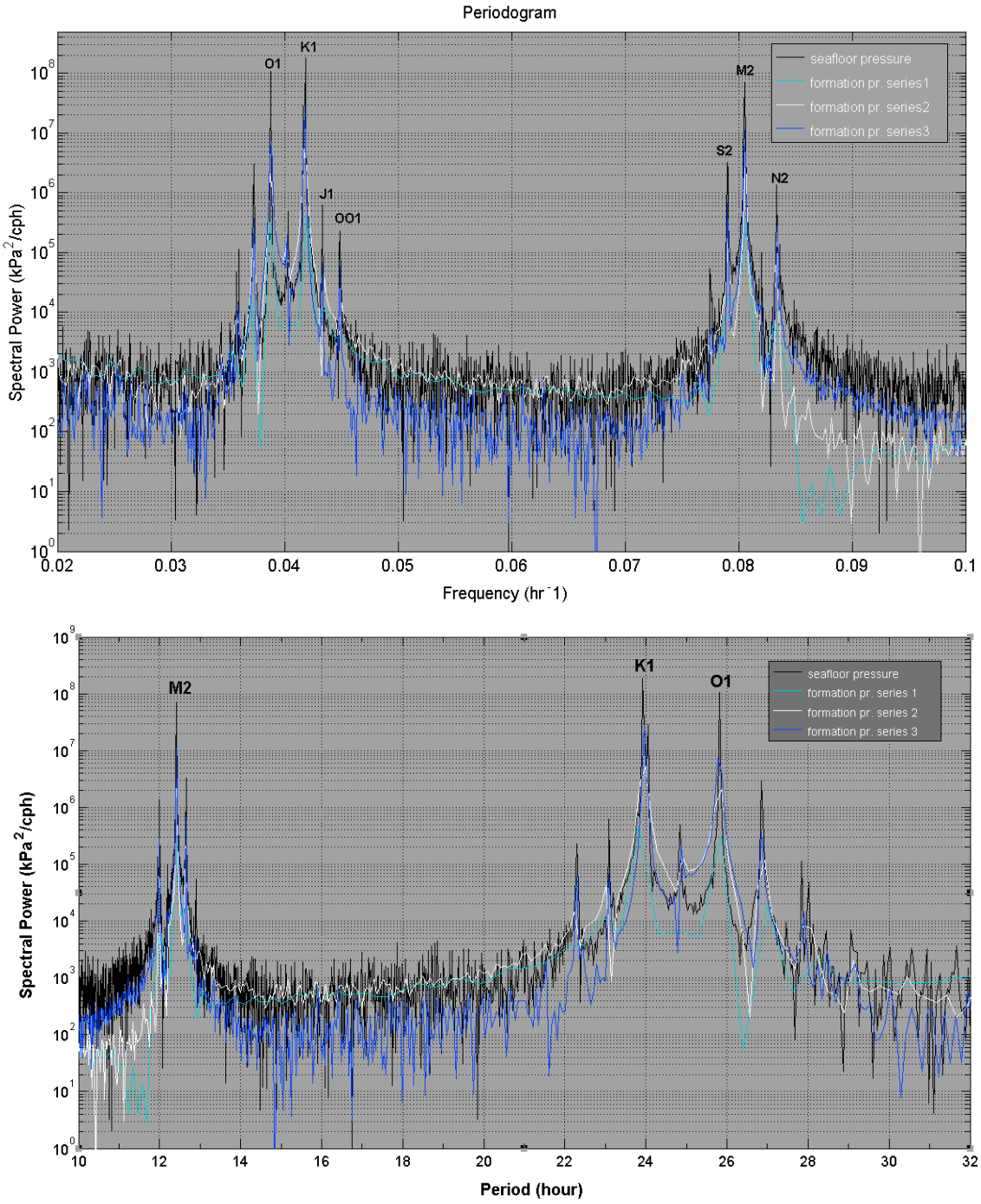

Figure 3.1: Typical power spectra for: 2-year seafloor pressure records, formation pressure *series 1* (118 days), *series 2* (165 days) and *series 3* (234 days) from borehole 1200C, showing important tidal constituents. Tidal constituent diurnal K1 has the greatest power, followed by O1 and semidiurnal M2.

3.2 Bulk Modulus of the Matrix Frame

Bulk modulus of the matrix frame is one of the parameters needed to calculate the permeability. Frame bulk modulus is inferred from the loading efficiency (see **section 2.1 equation 1** and **2**). Loading efficiency is comparable with amplitude ratio. Therefore, in order to compare with the theoretical characteristics of the signal propagation into the formation, we need to plot the observed amplitude ratios against the dimensionless depth (see **equation 7**). To calculate dimensionless depth for each tidal period, we need to know the distance of the signal propagation (d) and hydraulic diffusivity.

In this case, the distance of the signal propagation (d) is considered as 176 meter, because we assumed the propagation pathway of the signal is from the boundary (seafloor) until the average depth of open/screened borehole (176 mbsf). However we haven't got the number for hydraulic diffusivity yet, because loading efficiency is actually needed in order to accurately constraint the hydraulic diffusivity (discussed in the next section). Therefore, we plotted the amplitude ratio against the distance of the signal propagation and period neglecting the hydraulic diffusivity ($\zeta' = d/T^{1/2}$). Nevertheless, the data that were plotted in this manner follow a pattern that is similar in form to the predicted behavior as can be seen in **Figure 3.2.** When superimposed with the digitized type curves from Wang & Davis, the observed amplitude ratios were plotted close to the type curve of loading efficiency = 0.9.

We found that the amplitude ratios are clustered around 0.82 to 0.88 when they were plotted with more detailed scale **(Figure 3.3)**. For the calculation, we

use the median 0.85 for loading efficiency (**γ**). This high number of loading efficiency indicates that the matrix frame of the rocks in this formation is relatively more compressible, meaning that the fluids inside the pores take the greater share of the ocean tidal loads and therefore having a change in fluid pressure (formation pressure).

Using this loading efficiency and data of other formation properties in **Table 1.2** for **equation (1)** as described in **section 2.1**, the one dimension bulk modulus of matrix frame is 0.652 GPa or the compressibility of the matrix frame is 1.534 GPa^{-1}. The effective compressibility of this formation therefore can be calculated considering all bulk moduli of rock components (matrix frame, solid constituents and fluid) as described in **equation (4)** to be 1.25 GPa^{-1}.

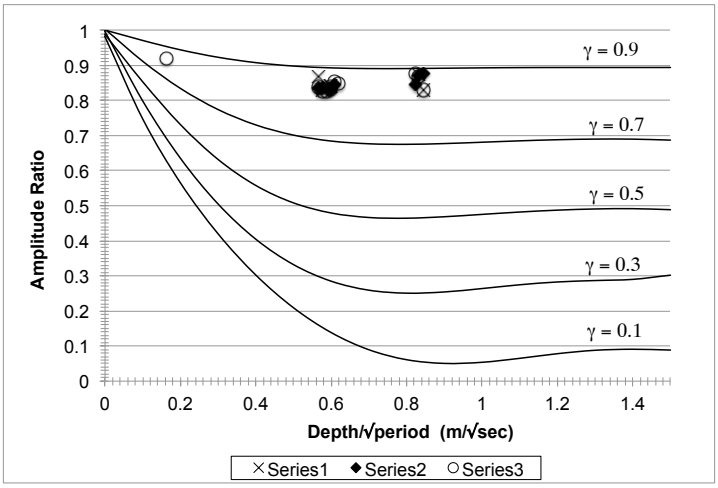

Figure 3.2: Plot of amplitude ratio versus depth of pressure propagation per square root of period. Data are superimposed on digitized type curve of theoretical model developed by Wang and Davis, 1996. It should be noted that the actual type curve in Wang & Davis (1996) has different x-axis properties with the plot. The x-axis for the type curve is dimensionless propagation length of the signal that includes the hydraulic diffusivity (see **Figure 2.3**)

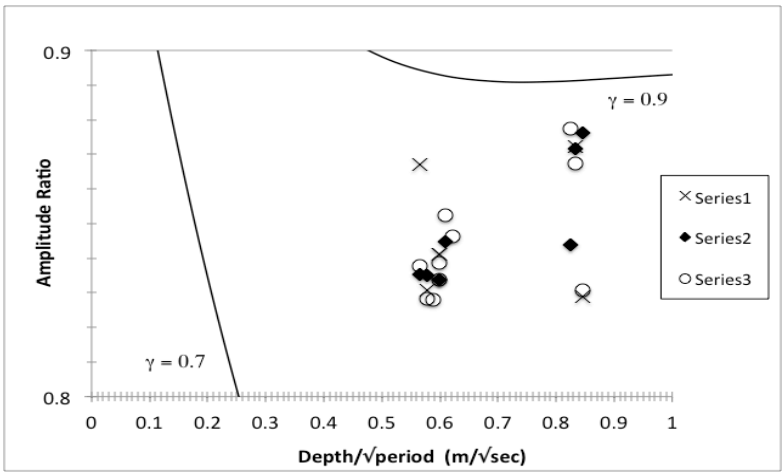

Figure 3.3: Plot of amplitude ratio versus depth of pressure propagation per square root of period (detail scale).

3.3 Permeability

In order to infer the permeability value, the hydraulic diffusivity needed to be calculated, which is based on their relationship in **equation (3).** The hydraulic diffusivity governs the length of the propagation of the pressure signal as described in **equation (6)**. The zero crossing of the phase difference data plotted in the type curve from Wang & Davis is used to deduce the propagation length as described in **section 2.1.** Because we already assumed the propagation length (d = 176 m), therefore we will use it to infer the hydraulic diffusivity. If we see the data in table 3.1, the phase differences that are very close to zero are at 24 hours period (P1 constituent). Using 24 hours as period (T) for the **equation (6)**, the hydraulic diffusivity was calculated to be 0.114 m^2/s.

By including this calculated hydraulic diffusivity into **equation (7)**, we can calculate the dimensionless depth for each period of tidal signals. If we plot dimensionless depths against the amplitude ratios (**Figure 3.4**), we found it still consistent with the behavior showing in Wang & Davis plot in **Figure 2.3.** For

plotting the dimensionless depths against the phase differences (**Figure 3.5)**, we found it also consistent with the behavior showing in Wang & Davis plot in **Figure 2.4** (note that the zero phase crossing is at dimensionless depth of 1). These phase differences were also plotted in more detailed scale as shown in **Figure 3.6**.

The resultant permeability value is 1.42 x 10^{-13} m^2 over the formation-scale of 176 meter from borehole. If we use the range of loading efficiency 0.82 to 0.88 instead of the median value of 0.85, we obtained a range of permeability, which is about 1.18 to 1.79 x 10^{-13} m^2. The uncertainties that come from other parameters used for the calculation, as shown in **Table 1.2**, would increase the uncertainty of this resultant permeability value. The calculation is summarized in **Table 3.2**.

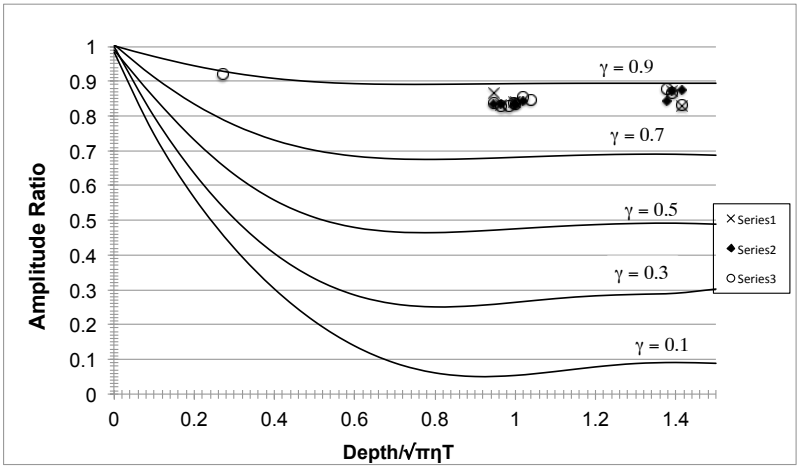

Figure 3.4: Plot of amplitude ratio versus dimensionless depth. Dimensionless depth of pressure propagation using calculated hydraulic diffusivity as described in text. Data are superimposed on digitized type curve of theoretical model developed by Wang and Davis, 1996.

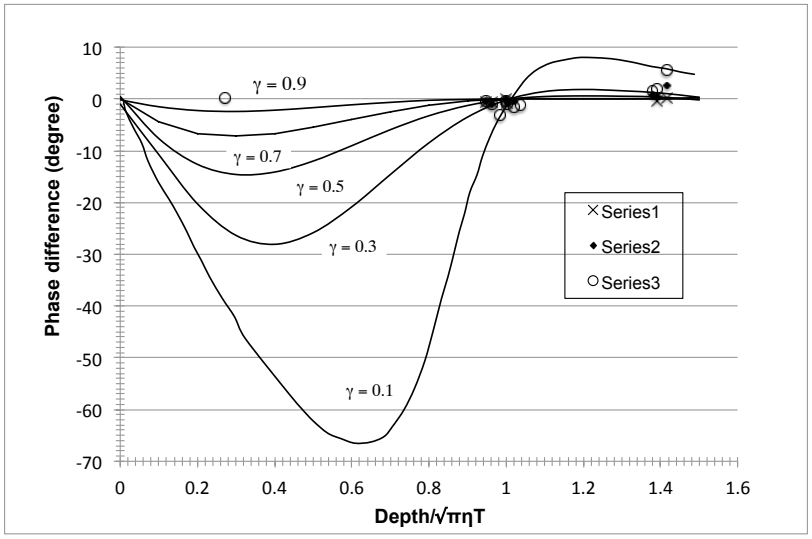

Figure 3.5: Plot of phase difference versus dimensionless depth of signal propagation. Data are superimposed on digitized type curve of theoretical model developed by Wang, et al., 1996.

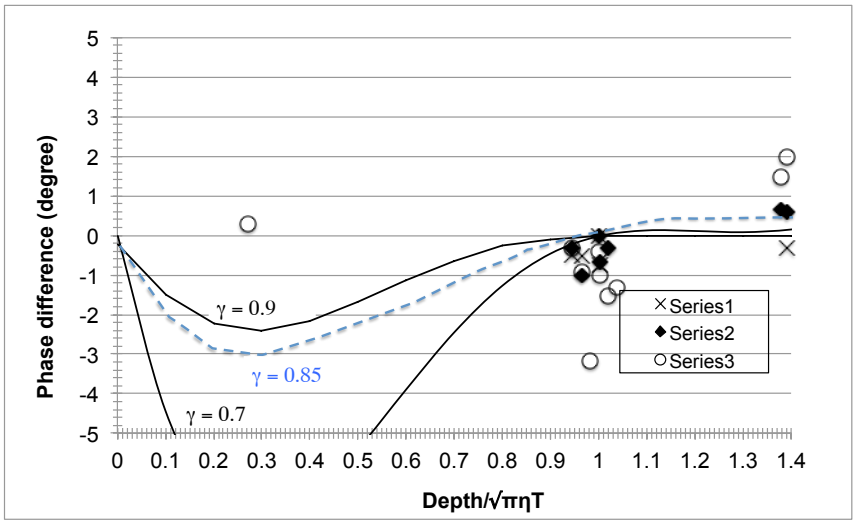

Figure 3.6: Plot of phase difference versus dimensionless depth of pressure propagation (detail scale). Dashed curve is an approximation for loading efficiency = 0.85.

3.4 Earthquake Effect

From **Table 3.1** we see that tidal response before and after the earthquakes as represented by the three different series show only very subtle differences, suggesting that the earthquake did not change the permeability.

Table 3.2: Characteristic of Elastic and Hydraulic Properties of South Chamorro Seamount Calculated using Tidal Method

No	Property	Sym-bol	Value			Unit	Source or Equation used
			Low	Median	High		
1	Loading efficiency	γ	0.82	0.85	0.88		Amplitude ratio profile
2	Bulk modulus of matrix frame (1-Dimension)	K'	1.171	0.941	0.727	GPa	$\gamma = \frac{1}{1 + n(\frac{K'}{Kf})}$ equation (1) $K' = \left(\frac{1}{\gamma} - 1\right)\frac{Kf}{n}$
3	Bulk modulus of matrix frame	K	0.811	0.652	0.503	GPa	$K' = 3K\frac{(1-v)}{(1+v)}$ equation (2) $K = \frac{K'(1+v)}{3(1-v)}$
4	Parameter elasticity	α			0.952		$\alpha = 1 - \frac{Kf}{Ks}$..... equation (5)
5	Effective compressi-bility	S	1.037	1.25	1.57	1/ GPa	$S = \left(\frac{1}{K} - \frac{1}{Ks}\right)\left(1 - \frac{2\alpha(1-2v)}{3(1-v)}\right) + n\left(\frac{1}{Kf} - \frac{1}{Ks}\right)$ equation..(4)
6	Hydraulic diffusivity	η			0.114 (T=24 hours)	m^2/s	$q = \sqrt{\pi \eta T}$ ..... equation (6) $\eta = \frac{(\frac{q}{\sqrt{T}})^2}{\pi}$
7	Permeability	κ	1.18 x10^{-13}	1.42 x10^{-13}	1.79 x10^{-13}	m^2	$\eta = \frac{\kappa}{\mu S}$... equation (3) $\kappa = \eta \mu S$

However, to see the earthquake effect more correctly, we performed the harmonic analysis for 29 days interval. Harmonic analysis requires the series length minimum of 29 days. A *synodic* month of 29 days is the average interval between corresponding phases of the moon, an interval significant for analysis purposes because it approximates a time when the major tidal constituents each complete a whole number of cycles (*Boon, 2007*). We made 29 groups which first group started from the beginning date until the end date of the hourly pressure data that made one group has about 23 series of 29 days interval. The next group started the next day, therefore from one group to the next group has 24

hours different. The result for each group shown the strongest amplitude was the K1 constituent, and followed by O1 and M2 constituent. Having combined the results from 29 groups, as we plotted the amplitude ratio and phase difference of K1 constituent against the mid point of each series of 29 days interval shown in **Figure 3.7** and **Figure 3.8**, we found some different results for each group. Because of these differences, we then calculated the average for the amplitude and phase of each seafloor and formation pressure data from these 29 groups for every single day, made it a moving average.

From the result of the moving average, plot of the amplitude ratio and phase difference of K1 constituent against each day were then made as shown in **Figure 3.9** and **Figure 3.10**. We could see from **Figure 3.9** that the amplitude ratio of K1 constituent changed at the time of earthquake, and in less than a month they went back to the previous state. For the phase difference of K1 constituent, the changes were more scattered and were not clearly seen happened at the time of earthquake. The anomalous change of the phase differences occurred at times other than the occurrence of the two-recorded earthquakes (**Figure 3.10)**.

We found that there are some earthquakes other than the two noticeable earthquakes that coincide with the rise in pressure data, happened during the two years observation around 500 km radius from the borehole 1200C. These earthquakes happened in April, June and August in the year 2001, and in February, March, May, August, October and November in the year 2002 and in January 2003 (Data from International Seismological Centre, 2011, summarized

by Vinas, 2013, see **Appendix**). These earthquakes may be the cause of the anomalies, since almost all of them coincide with these anomalous changes. However, we could not find the good explanation as to why these earthquakes did not appear as the pressure rise in the pressure data.

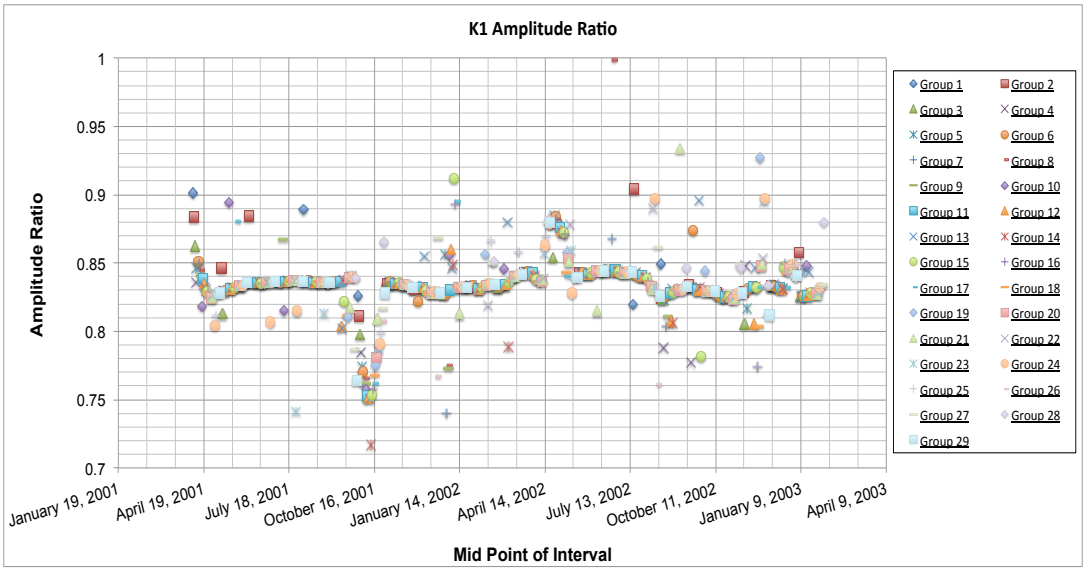

Figure 3.7: Amplitude ratio of formation tidal signal K1 relative to seafloor loading, calculated for 29-day window plotted at mid point of each interval. 29 groups was made and shown difference between groups.

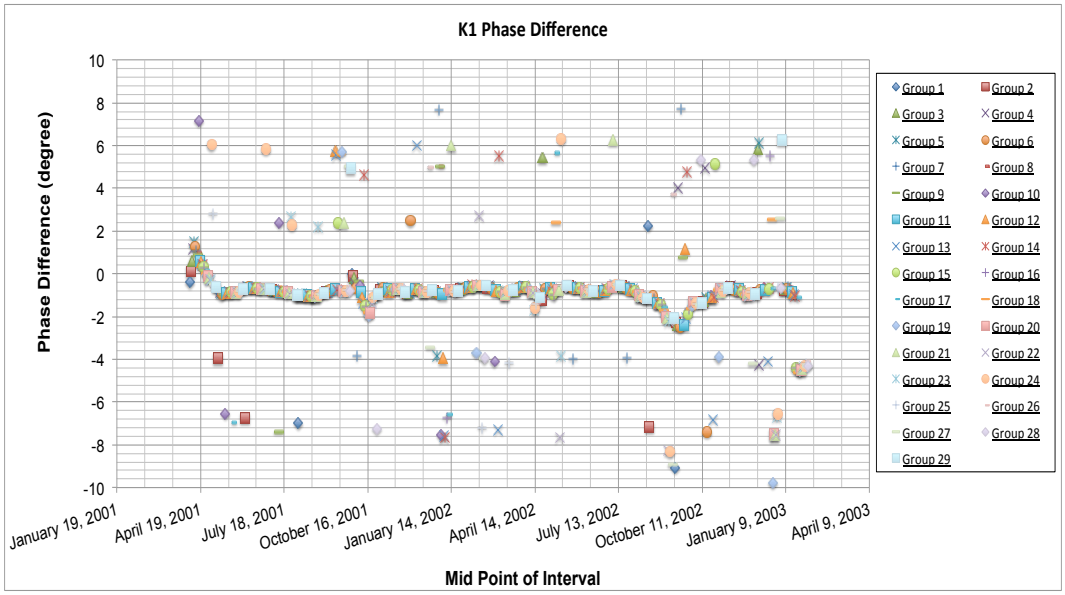

Figure 3.8: Amplitude ratio of formation tidal signal K1 relative to seafloor loading, calculated for 29-day window plotted at mid point of each interval. 29 groups was made and shown difference between groups.

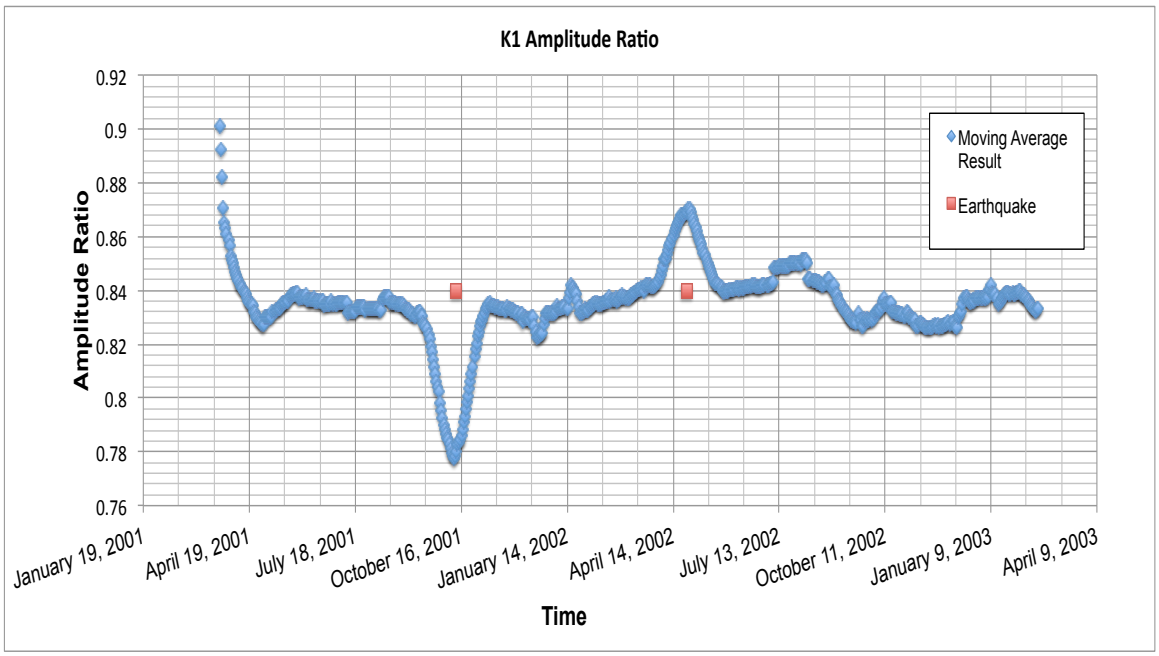

Figure 3.9: Amplitude ratio of K1 tidal constituent, calculated for 29-day window. Points of each day are resulted from moving average. Effect from drilling perturbation, which is shown as anomalous curve, from early time until around June 2001, can be ignored. The two red blocks are only the marks to show the time of the two big earthquakes and do not represent the amplitude ratio at those times. Sudden jump or fall of the amplitude ratio occurred at the time of these two big earthquakes.

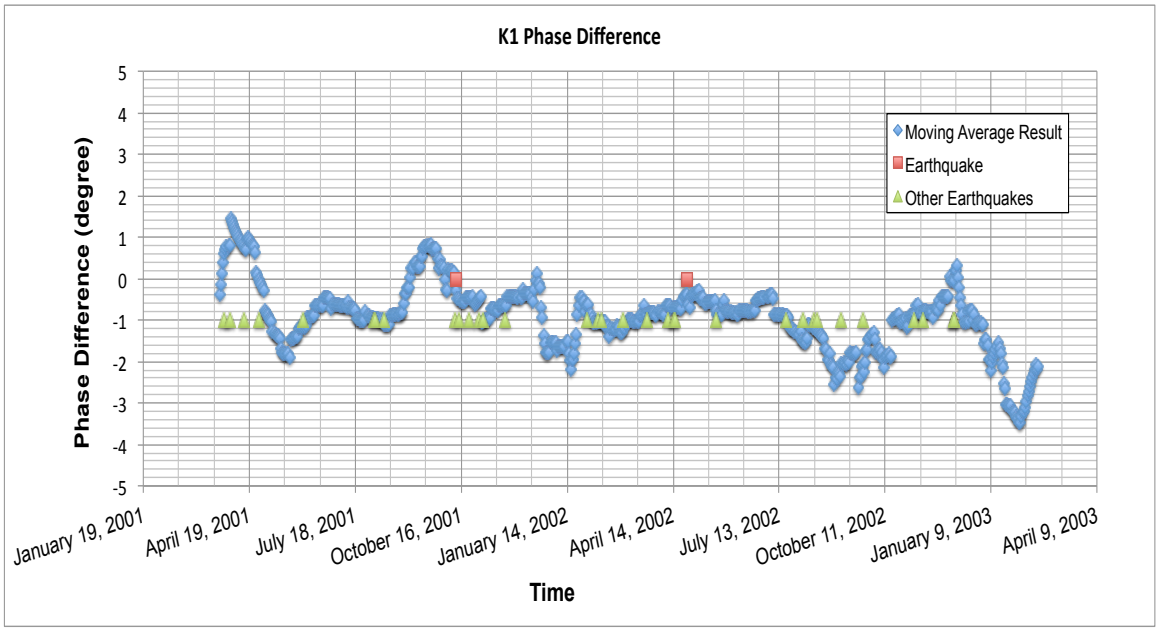

Figure 3.10: Phase difference of K1 tidal constituent, calculated for 29-day window. Points of each day are resulted from moving average. The two red blocks and several green triangles are only the marks to show the time of the earthquakes and do not represent the phase difference at those times. Phase differences change at the time of these earthquakes.

We also noticed that at the time of the first earthquake (October 12, 2001), the strongest amplitude was not the K1 constituent, but the O1 and M2. When we plot the amplitude of these tidal constituents, K1 constituent shown highly sinusoidal wave compared to other constituents (**Figure 3.11**). This undulation happened every six months and the formation amplitude was at around 1 kPa at the time of earthquake happened.

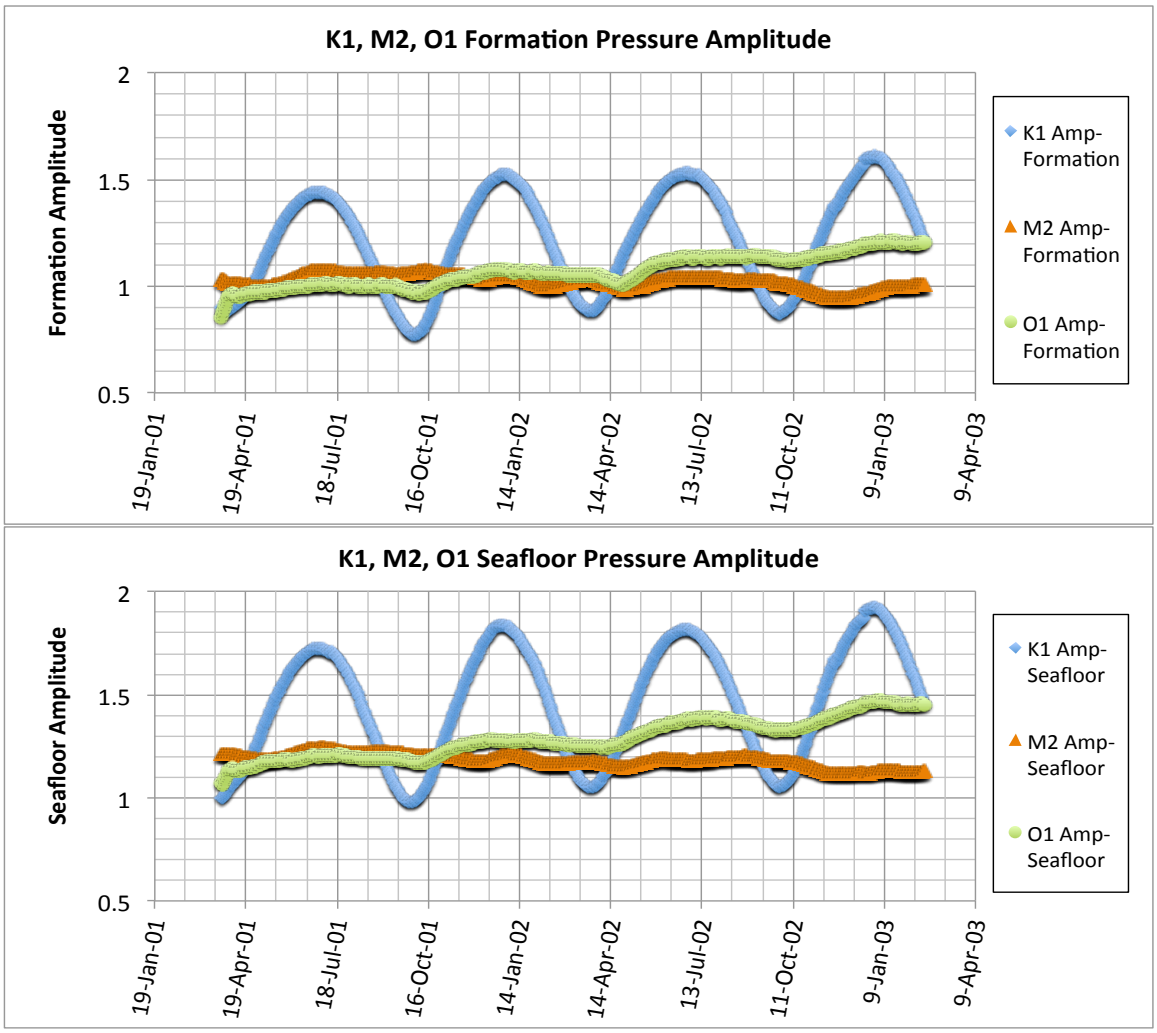

Figure 3.11: Amplitude of formation and seafloor tidal signals for the K1, O1 and M2 tidal constituent, calculated for 29-day window. K1 constituent shows highly sinusoidal wave.

Figure 3.12 below shown the amplitude ratio and phase difference for those tidal constituents and even though they have different pattern, we still could find that they changed at the time of two noticeable earthquakes that coincide with the rise in pressure data and rapidly back to normal, and some anomalous changes at the time of other earthquakes.

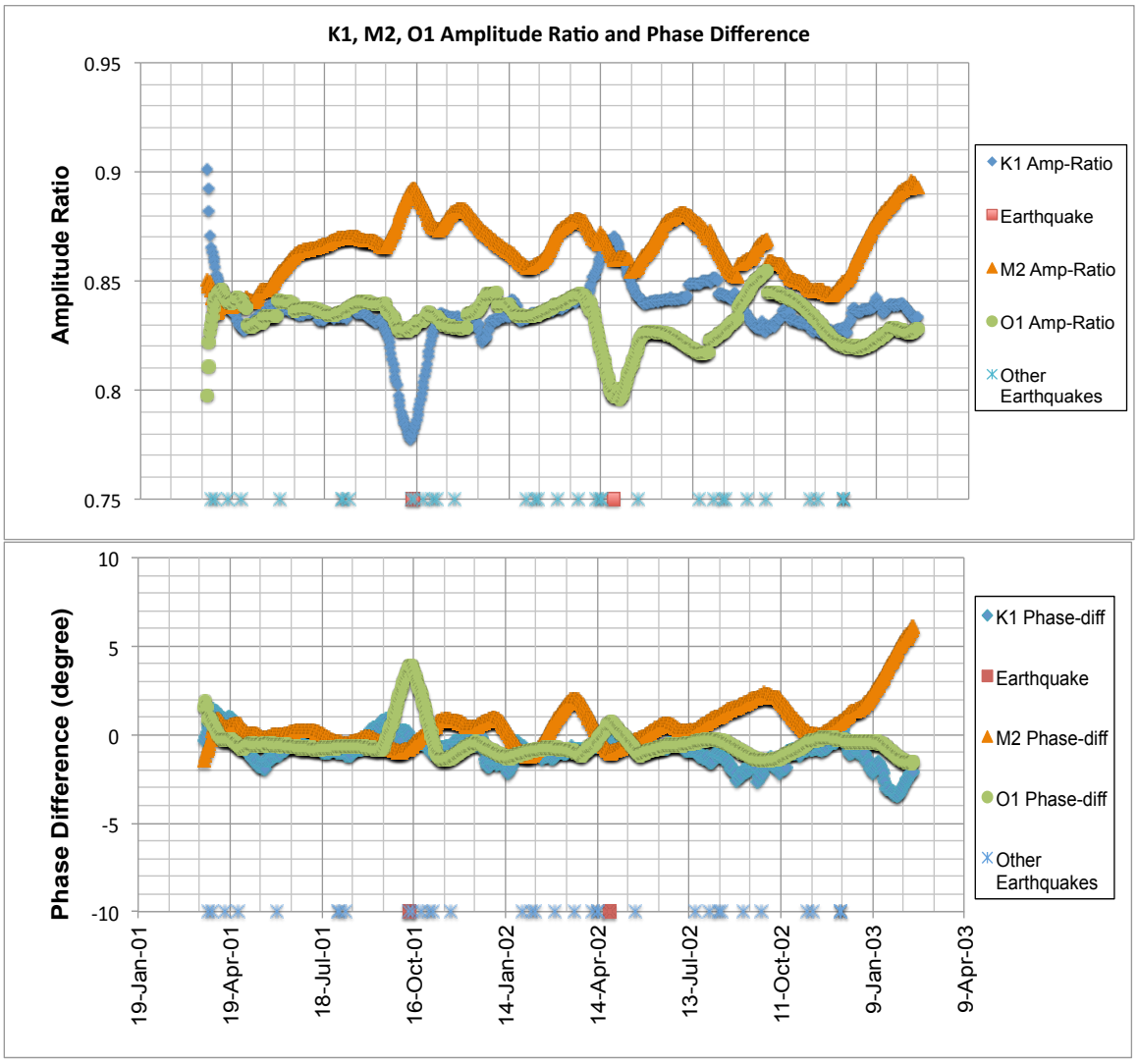

Figure 3.12: Phase and amplitude of formation tidal signals response for the K1, O1 and M2 tidal constituent relative to seafloor loading, calculated for 29-day window. The two red blocks and several blue stars are only the marks to show the time of earthquakes and do not represent the amplitude ratio or phase difference at those times.

3.5 Discussion

3.5.1 Comparison to Theoretical Model

The behavior of the results are consistent with the theory; near the boundary, relative amplitudes are large, approaching unity at low frequency, and phases are relatively small, and as it goes further the amplitudes decrease and phase becomes more negative with increasing frequency and becomes positive as the half wavelength of the signals were reached. However, the agreement is not perfect, as we see the positive phases beyond the zero-phase crossing are larger than predicted theoretically (**Figure 3.6**). The inaccuracy in digitizing the theoretical type curve may contribute to this discrepancy. The phase of the formation signals that shifted just a little from the seafloor loading and are located at the penetration depth and afterwards, suggests that the pore pressure changes were primarily elastic. This condition raises a question about the diffusive pressure signal, whether the tidal signal diffuses with the assumed propagation path, i.e. from the seafloor trough the 176-meter of sediment, is possible or might follow a different path. We still could not find a good explanation for this behavior and could not suggest for the possible alternative propagation path for the diffusive signal.

Furthermore, assuming the crust as a medium with uniform and isotropic properties is maybe too simplistic, as the variations in fracture and alteration will contribute to heterogeneity and anisotropy and permeability distribution (Davis et al, 2000). The more complex investigation concerning this issue requires more detailed data and experiments. Nevertheless, with this simple model, elastic

property (frame bulk modulus) and hydraulic property (permeability) of the formation can be estimated. From the resultant high number of loading efficiency we could infer that characteristic of the matrix frame of serpentine blueschist rock is compressible, with bulk modulus 0.652 ± 0.15 GPa.

3.5.2 Permeability value

There were other techniques used to calculate permeability of the seamount at or near Hole 1200C. The laboratory core-based method was applied for core samples from Pacman Seamount. In this method, the sample was placed inside a uniaxial floating-ring back pressured consolidometer and vertical stresses from 25 to 3200 kPa were applied to imitate 400-500 m burial. Fluid was pumped to flow across the sample and pressure differences across each sample were then measured. By using Darcy's Law equations, permeability needed to sustain the rate of flow under that condition can be calculated. For blue-mud sample, the permeabilities calculated with range from 10^{-17} m^2 to 10^{-15} m^2 (Wheat et al., 2008).

Another method used for estimating permeability is by measuring the rate of fluid flow which occurred at borehole depth when the CORK was removed in Hole 1200C. The flow rate of discharge and excess formation pressure measured in situ were then combined with time of flow, thickness of the open borehole, porosity, viscosity, and fluid compressibility in a radial diffusion equation to calculate permeability. The permeability calculated using this method is 6 $x10^{-14}$ m^2, which is required to allow the observed rate of flow of 0.08 ± 0.04 L/s (Wheat et al, 2008). The probable reasons for the difference in permeability

value using these two different methods were explained by Wheat et al (2008) to be: 1) the scale of fluid flow in core-samples did not represent the cracks and fractures that are likely to be the pathway for large-scale fluid migration and 2) core-based uniaxial measurement only measure vertical permeability, whereas from borehole the horizontal component is included. Therefore, permeability using in-situ measurements represents a larger portion of the interconnected pore in the formation than the core-based method.

In this study, the resultant permeability using tidal-loading method is also greater than the permeability of the core-based method. Therefore, the first hypothesis is proven; that the estimated value of permeability using data from in-situ measurement would be greater and more representative of large-scale formation permeability than the core-based measurement. The resultant permeability, i.e. 1.42×10^{-13} m^2, is higher than the borehole flow method. The difference of the value with the borehole flow method might show a scale-dependence of permeability as commonly observed in permeabilities measured in crystalline rocks with different method that are ranging in measurement scales (Becker and Davis, 2003). To be able to confirm this scale-dependence, it might be required to drill the borehole deeper or use other borehole methods, but attempts to drill deeper into this formation were already unsuccessful. However, the value is in the same order with the value estimated by Wheat using radial diffusion equation for the case of formation fluid ascending through a 5-meter thick fault zone, i.e. 6×10^{-13} m^2. Because the scale of investigation for the permeability by tidal loading method is 176 meter, it would encompass such a

fault zone. However, the fault zone itself might have greater permeability than this resultant bulk permeability. This assumption cannot be validated until more information about the detailed structure of this formation is collected.

3.5.3 Earthquake Effects on Permeability value

The amplitude ratio and phase difference changed at the time of earthquake, as has been observed in oceanic crust, which suggests sensitivity of elastic and hydrologic properties to strain. Even though the cause of this sensitivity is not well understood, Davis and Becker (2004) suggest that it may be associated with strain amplification by fractures or faults. However, we found that the changes have different behavior, as they return to normal state very rapidly; they need less than a month compared to many months needed by the oceanic crust (**Figure 2.5**). We could infer that this different behavior is based on the difference in material forming each crustal type; the forearc crust with more homogeneous and mostly finer mixed metamorphic-sedimentary type of material is more elastic than the oceanic crust with the two-layer sediment and igneous basement rocks.

CHAPTER 4

CONCLUSION

The Circulation Obviation Retrofit Kit (CORK) installed in ODP borehole observatory 1200C provides a way to characterize the blueschist serpentinite formation in the forearc crust. Formation pressure data from this borehole show a record that is dominated by tidal influences with two transient pressure increases that occur at the time of two large earthquakes around the area. The strongest tidal constituent in this area is the *luni-solar diurnal* constituent or *K1*, which has tidal period of 23.93 hours. The fluctuation pressure response to tidal loading makes these data suitable to calculate permeability using the tidal loading method. Assuming the crust is a uniform and isotropic medium, and propagation pathway is from the seafloor through the 176-meter of sediment, the bulk permeability is calculated to be 1.42×10^{-13} m^2, for the scale of investigation of about 176 meters both vertically from the seafloor and laterally from the borehole. This estimated value of permeability using data from in-situ measurement is greater and more representative of large-scale formation permeability than the core-based measurement.

Characteristic of the matrix frame of serpentine blueschist rock of the seamount is compressible, with bulk modulus of 0.652 ± 0.15 GPa. Tectonic activity would not change or enhance the formation permeability. This is because of the amplitude ratio and phase difference changed instantaneously at the time of earthquake, that may be caused by amplification of strain by fractures or faults, and then return to their normal state in less than a month, suggest that this

forearc crust has more elastic behavior compare to the oceanic crust. The more homogeneous and mostly finer mixed metamorphic-sedimentary type of material composition may be the cause for this behavior.

Furthermore, this study could be improved by collecting more information about the detail structure of the formation, in order to be able to answer some questions which arose during the observation of the result from the analysis done in this study, which mostly caused by assuming the crust as a medium with uniform and isotropic properties and having the propagation pathway of the diffusive signal to be around 176-meter of sediment from the seafloor.

REFERENCES

Becker, K. and E. Davis, 2003. New evidence for age variation and scale effects of permeabilities of young oceanic crust from borehole thermal and pressure measurements. *Earth and Planetary Sci. Lett.* 210: 499-508.

Becker, K. and E. Davis, 2004. In situ determinations of the permeability of the igneous oceanic crust. In *Hydrogeology of the Oceanic Litosphere*: Cambridge University Press, 189-226.

Becker, K. and E. Davis, 2005. A review of CORK designs and operations during the Ocean Drilling Program. In Fisher, A.T., Urabe, T., Klaus, A., and the Expedition 301 Scientists, *Proc. IODP, 301*: College Station, TX (Ocean Drilling Program), 1-28.

Biot, M.A., 1962. Mechanics of deformation and acoustic propagation in porous media. *Journal of Applied Physics* 33, no 4: 1,482-1,498.

Boon, J.D, 2004. Secrets of the tide: tide and tidal current analysis and predictions, storm surges and sea level trends. Horwood Publishing, Chichester, U.K., 153-156.

Boon, J.D., 2007. World Tides User Manual version 1.03.

Bredehoeft, J.D. and S.S. Papadopulos, 1980. A method for determining the hydraulic properties of tight formations. *Water Resources Research* **16**(1): 233-238.

Courtier, A.M., Hart, D.J., and Christensen, N.I. 2006. Seismic properties of Leg 195 serpentines and their geophysical implications. In *Proc. ODP, Sci. Results*, 195 *Initial Reports*, 195: College Station, TX (Ocean Drilling Program), 1-12 [CD-ROM].

Davis, E.E., Wang, K., Becker, K., and Thompson, R.E., 2000. Formation-scale hydraulic and mechanical properties inferred from pressure response to periodic seafloor loading. *J. Geophys. Res*. 105: 13,423-13,435.

Elderfield, H., Becker, K., and Davis, E.E., 2004. Foundations of research into heat, fluid, and chemical fluxes in oceanic crust. In *Hydrogeology of the Oceanic Litosphere*: Cambridge University Press, 28-56.

Fisher, A.T., 2005. Marine Hydrogeology: recent accomplishments and future opportunities. *Journal of Hydrogeology* 13: 69-97.

Fryer, P. 1996, Tectonic evolution of the Mariana convergent margin, *Rev. Geophys.,* 34: 89–125.

Fryer, P., Gharib, J., Ross, K., Savov, I., and Mottl, M., 2006. Variability in serpentine mudflow mechanisms and sources: ODP drilling results on Mariana forearc seamounts, *Geochem. Geophys. Geosyst.,* 7, no 8: 1-15.

Fryer, P.B., and M.H. Salisbury, 2006. Leg 195 synthesis: Site 1200—serpentinite seamounts of the Izu-Bonin/Mariana convergent plate margin (ODP Leg 125 and 195 drilling results). *In* Shinohara, M., Salisbury, M.H., and Richter, C. (Eds.), *Proc. ODP, Sci. Results,* 195: College Station TX (Ocean Drilling Program), 1–30.

Fryer, P. 2012, Serpentinite mud volcanism: observations, processes, and implications. In C. A. Carlson and S. J. Giovannoni, *Annual Review of Marine Science,* Vol 4: 345-373.

Hamilton, E.L., 1971. Elastic properties of marine sediments. *J. Geophys. Res*. 76, no.2: 579-604.

Inderbitzen, K.E., 2013. Analysis of long-term borehole and seafloor pressure data recorded by the subseafloor observatories in Middle Valley, Northern Juan de Fuca Ridge. *University of Miami Open Access Dissertations.* Paper 1017.

International Seismological Centre, *On-line Bulletin*, http://www.isc.ac.uk, Internatl. Seis. Cent., Thatcham, United Kingdom, 2011.

Kamp, G. and J.M. Gale, 1983. Theory of earth tide and barometric effects in porous formations with compressible grains. *Water Resources Res*., 19, no.2: 538-544.

Oakley, A.J., Taylor, B., Fryer, P., Moore, G.F., Goodliffe, A.M., Morgan, J.K., 2007, Emplacement, growth, and gravitational deformation of serpentinite seamounts on the Mariana forearc. *Geophys. J. Int,* 170: 615-634.

Pawlowicz, R., B. Beardsley, and S. Lentz (2002), Classical tidal harmonic analysis including error estimates in MATLAB using T-TIDE, *Computers & Geosciences*, 28(8): 929–937.

Salisbury, M.H., Shinohara, M., Richter, C., et al, 2002. Leg 195 summary. In *Proc. ODP, Initial Reports*, 195: College Station, TX (Ocean Drilling Program), 1-63.

Salisbury, M.H., Shinohara, M., Richter, C., et al, 2002. Site 1200. In *Proc. ODP, Initial Reports*, 195: College Station, TX (Ocean Drilling Program), Chapter 3 [CD-ROM].

Shinohara, M., Salisbury, M.H., Richter, C., et al., 2006. Proceedings of the Ocean Drilling Program, *Scientific Results* 195: College Station, TX (Ocean Drilling Program).

Tidal Analysis Program in Python, Timcera, 2012. http://sourceforge.net/apps/mediawiki/tappy/index.php?title=TappyUsersGuide http://sourceforge.net/apps/mediawiki/tappy/index.php?title=CompareTidalFilters

Vinas, K.A., 2013. Mariana forearc crust CORK pressure data: observations and implications. *University of Miami Open Access Theses*. Paper 436.

Wang, K., and E.E. Davis, 1996. Theory for the propagation of tidally induced pore pressure variations in layered subseafloor formations. *Journal of Geophysical Research* vol. 101, no. B5: 11,483-11,495.

Wang, K. 2004. Applying fundamental principles and mathematical models to understand processes and estimate parameters. In *Hydrogeology of the Oceanic Litosphere*: Cambridge University Press, 376-413.

Wheat, G.C., Fryer, P., Fisher, A.T., Hulme, S., Jannasch, H., Mottl, M.J., Becker, K. 2008. Borehole observations of fluid flow from the South Chamorro Seamount an active serpentine and mud volcano in the Mariana Forearc. *Earth and Planetary Sci. Lett.* 267: 401-409.

APPENDIX

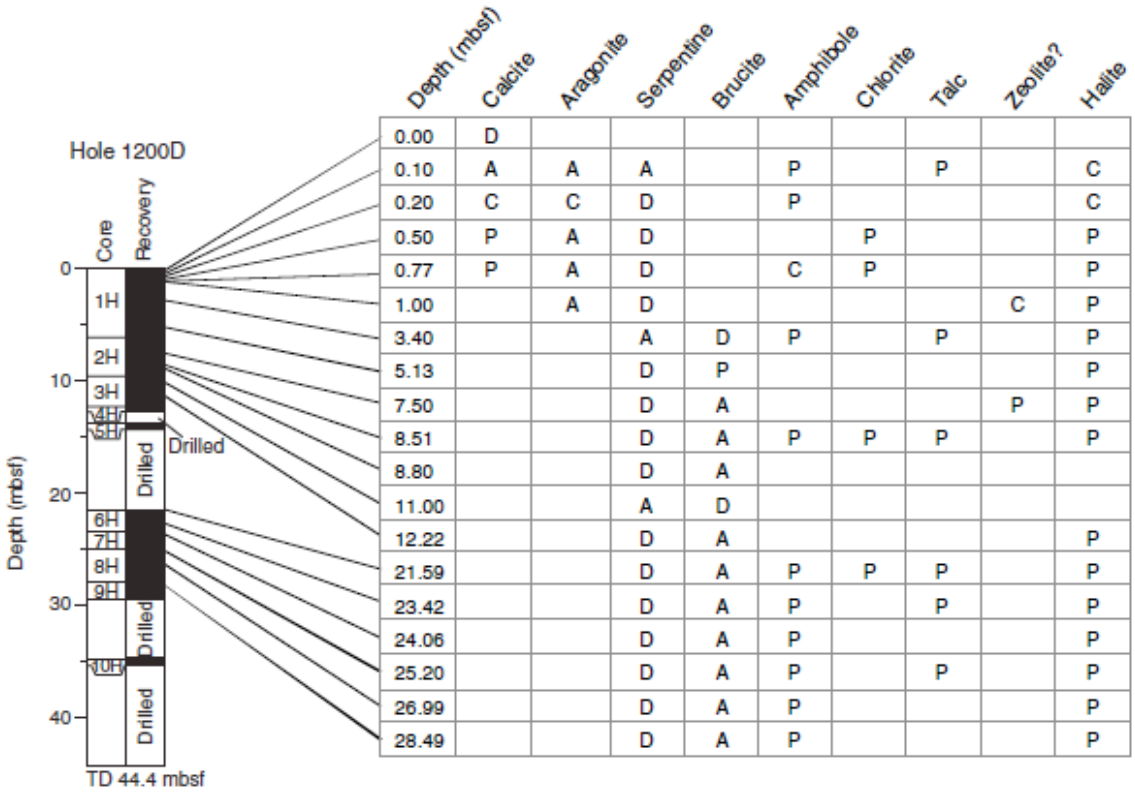

Depth (mbsf)	Calcite	Aragonite	Serpentine	Brucite	Amphibole	Chlorite	Talc	Zeolite?	Halite
0.00	D								
0.10	A	A	A		P		P		C
0.20	C	C	D		P				C
0.50	P	A	D			P			P
0.77	P	A	D		C	P			P
1.00		A	D					C	P
3.40			A	D	P		P		P
5.13			D	P					P
7.50			D	A				P	P
8.51			D	A	P	P	P		P
8.80			D	A					
11.00			A	D					
12.22			D	A					P
21.59			D	A	P	P	P		P
23.42			D	A	P		P		P
24.06			D	A	P				P
25.20			D	A	P		P		P
26.99			D	A	P				P
28.49			D	A	P				P

Figure 1: Downhole changes in semi-quantitative mineralogy of silty clay–sized serpentine in Hole 1200D, as inferred from XRD analyses of bulk powder mounts. Abundance: D = dominant (50%–100%), A = abundant (20%–50%), C = common (5%–20%), P = present (1%–5%). TD = total depth. Figure from Salisbury et al., 2002.

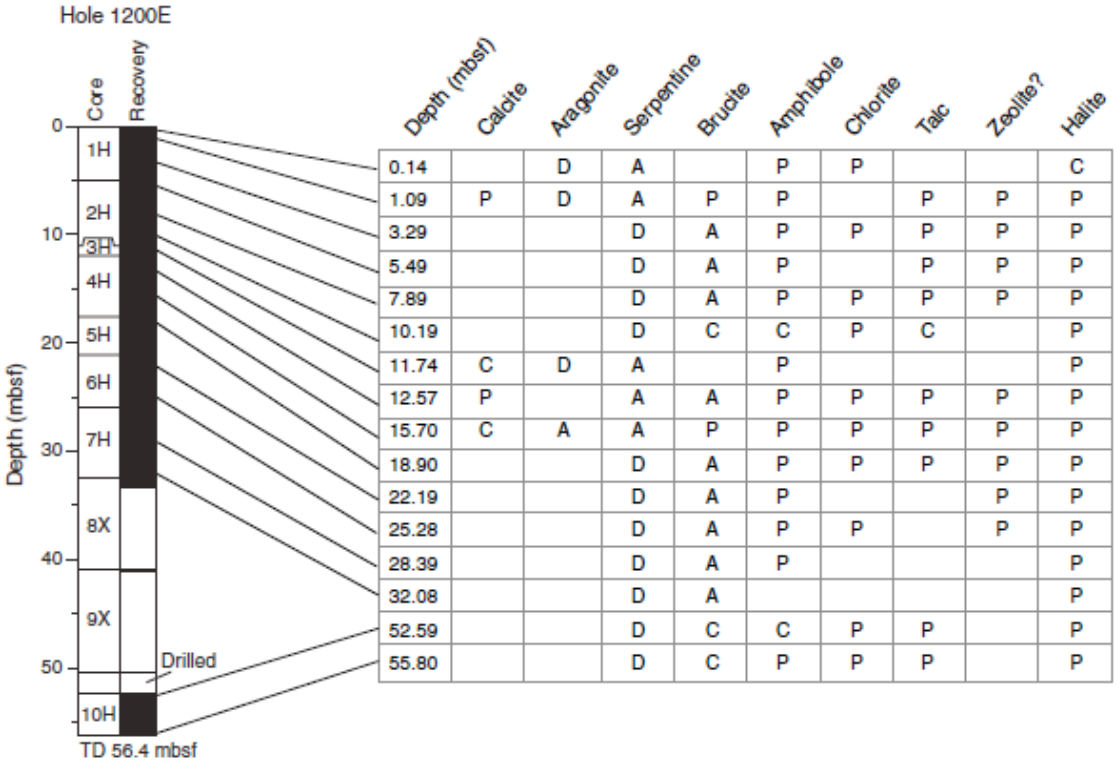

Depth (mbsf)	Calcite	Aragonite	Serpentine	Brucite	Amphibole	Chlorite	Talc	Zeolite?	Halite
0.14		D	A		P	P			C
1.09	P	D	A	P	P		P	P	P
3.29			D	A	P	P	P	P	P
5.49			D	A	P		P	P	P
7.89			D	A	P	P	P	P	P
10.19			D	C	C	P	C		P
11.74	C	D	A		P				P
12.57	P		A	A	P	P	P	P	P
15.70	C	A	A	P	P	P	P	P	P
18.90			D	A	P	P	P	P	P
22.19			D	A	P			P	P
25.28			D	A	P	P		P	P
28.39			D	A	P				P
32.08			D	A					P
52.59			D	C	C	P	P		P
55.80			D	C	P	P	P		P

Figure 2: Downhole changes in semiquantitative mineralogy of silty clay–sized serpentine in Hole 1200E, as inferred from XRD analyses of bulk powder mounts. Abundance: D = dominant (50%–100%), A = abundant (20%–50%), C = common (5%–20%), P = present (1%–5%). TD = total. Figure from Salisbury et al., 2002.

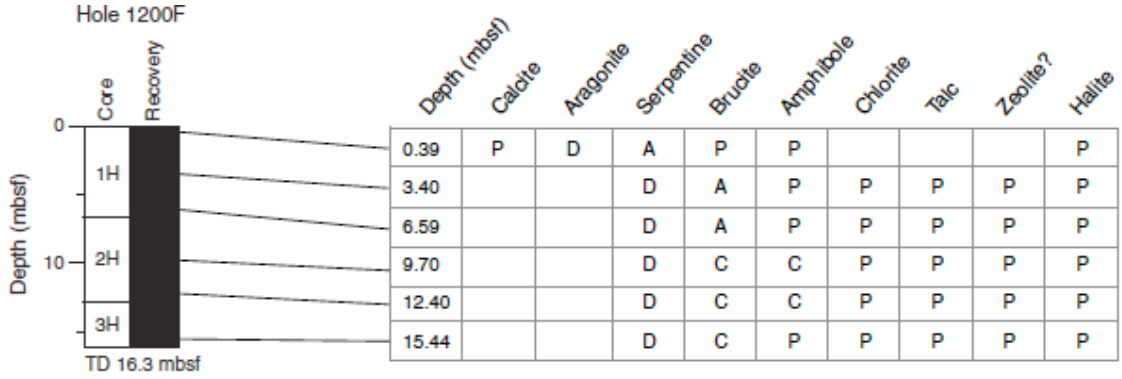

Depth (mbsf)	Calcite	Aragonite	Serpentine	Brucite	Amphibole	Chlorite	Talc	Zeolite?	Halite
0.39	P	D	A	P	P				P
3.40			D	A	P	P	P	P	P
6.59			D	A	P	P	P	P	P
9.70			D	C	C	P	P	P	P
12.40			D	C	C	P	P	P	P
15.44			D	C	P	P	P	P	P

Figure 3: Downhole changes in semi-quantitative mineralogy of silty clay–sized serpentine in Hole 1200F, as inferred from XRD analyses. Abundance: D = dominant (50%–100%), A = abundant (20%–50%), C = common (5%–20%), P = present (1%–5%). TD = total depth. Figure from Salisbury et al., 2002.

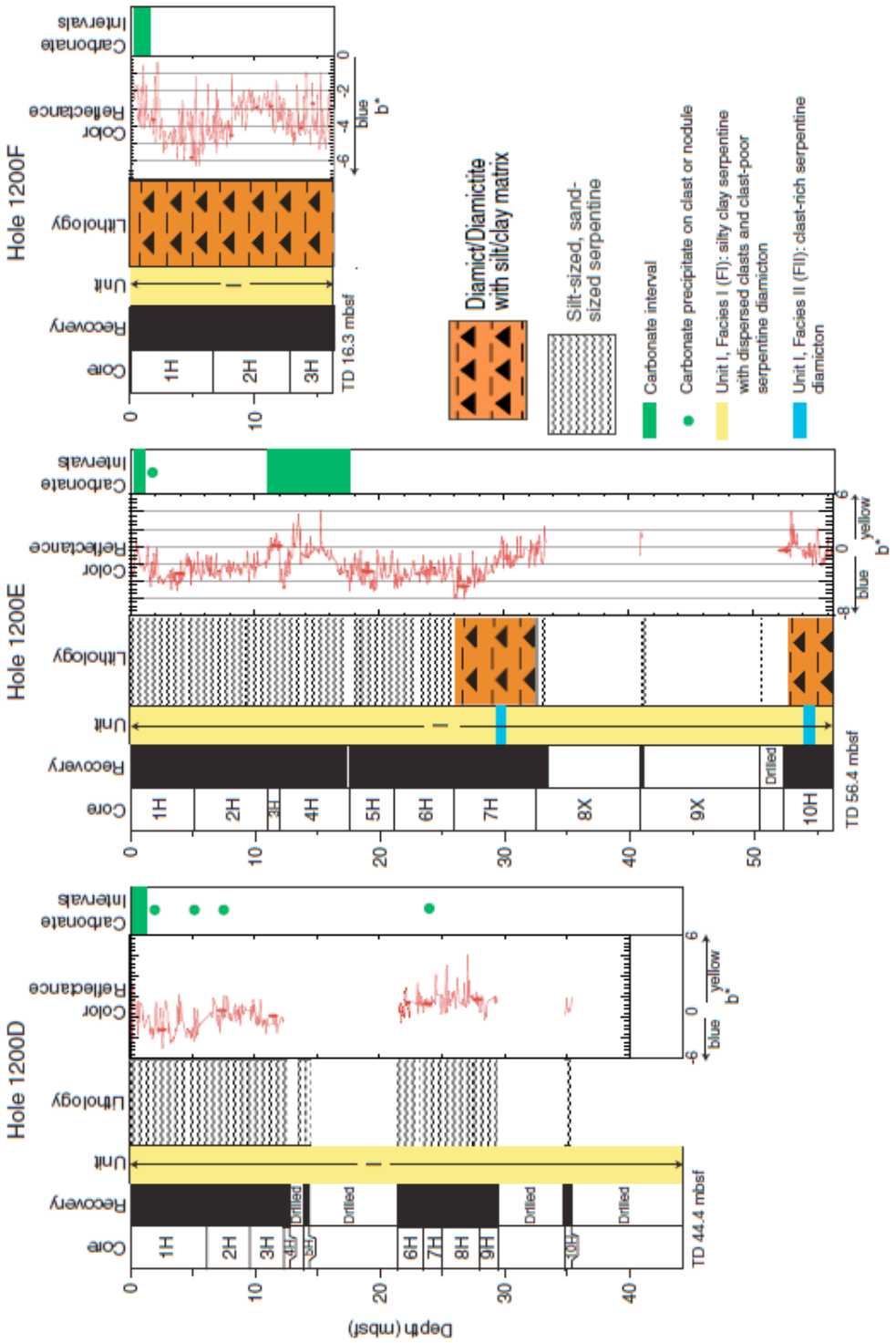

Figure 4: Summary figure for Site 1200 including lithology, color reflectance, and calcareous intervals. Yellow intervals in the "Unit" column indicate intervals of Facies I. Light blue intervals in the same column indicate intervals of Facies II.
TD = total depth. Figure modified from Salisbury et al., 2002

```
# You need to specify the separator between the integer part and the decimal

# part of real numbers, even if you only have integers in your data file.

decimal_sep = "."



# TAPPy needs the variables 'year', 'month', 'day', 'hour', 'minute',
'water_level'.

# Any other variable name can be used as a placeholder.

parse = [

          integer('recnum'),

          positive_integer('day', exact=2),

          positive_integer('month', exact=2),

          positive_integer('year', exact=2),

          positive_integer('hour', exact=2),

         positive_integer('minute', exact=2),

          positive_integer('second', exact=2),

          real('water_level'),

         real('seafloor'),

                                          ]
```

Figure 5: Data Definition File for Formation Pressure Data.

```
# You need to specify the separator between the integer part and the decimal

# part of real numbers, even if you only have integers in your data file.

decimal_sep = "."



# TAPPy needs the variables 'year', 'month', 'day', 'hour', 'minute',
'water_level'.

# Any other variable name can be used as a placeholder.

parse = [

          integer('recnum'),

          positive_integer('day', exact=2),

          positive_integer('month', exact=2),

          positive_integer('year', exact=2),

          positive_integer('hour', exact=2),

         positive_integer('minute', exact=2),

          positive_integer('second', exact=2),

          real('formation'),

         real('water_level'),

         ]
```

Figure 6: Example of Data Definition File for Seafloor Pressure Data.

Table 1: Harmonic Analysis Result for Formation Pressure Data Series 1.

```
(Canopy 32bit) Putris-MacBook-Pro:range1_n putriakmal$ ../tappy.py analysis
1200C_range1_n.txt data_def_fm.txt --linear_trend
#         NAME         SPEED             H         PHASE
#         ====         =====             =         =====
            Mm   0.54437433       0.3308     290.9083
           MSf   1.01589594       0.0989      47.7822
           2Q1  12.85428677       0.0382      60.3290
            Q1  13.39866110       0.1939     230.0829
            O1  13.94303543       0.9837      60.3107
           NO1  14.49669429       0.0078     345.2329
            K1  15.04106863       1.5382      77.8365
            J1  15.58544296       0.0782     282.2008
           OO1  16.13910182       0.0701     123.2229
          ups1  16.68347615       0.0038     336.5852
          MNS2  27.42383379       0.0098     149.2393
           mu2  27.96820812       0.0191     352.7252
            N2  28.43972973       0.2705     123.1312
            M2  28.98410406       1.0626     331.8872
            L2  29.52847839       0.0375     185.6830
            S2  30.00000000       0.1463     320.4965
          eta2  30.62651159       0.0126      90.5365
          2SM2  31.01589594       0.0062      48.8928
           MO3  42.92713949       0.0043      48.7787
            M3  43.47615609       0.0174     250.3261
           MK3  44.02517269       0.0122     213.5463
           SK3  45.04106863       0.0119      75.4876
           MN4  57.42383379       0.0049     323.2132
            M4  57.96820812       0.0265     197.7562
           SN4  58.43972973       0.0066     154.8497
           MS4  58.98410406       0.0041     231.2978
            S4  60.00000000       0.0060     275.0421
          2MN6  86.40793785       0.0051     337.7347
            M6  86.95231218       0.0016     182.0217
          2MS6  87.96820812       0.0002      53.9233
          2SM6  88.98410406       0.0006      47.9760
            S6  90.00000000       0.0062      88.2821
            M8 115.93641624       0.0014      31.9316
# INFERRED CONSTITUENTS
#         NAME         SPEED             H         PHASE
#         ====         =====             =         =====
          rho1  13.47151382       0.0374     209.2544
            M1  14.49205203       0.0698      59.2642
            P1  14.95893137       0.5091       7.4700
           2N2  27.89535540       0.0276      49.2082
           nu2  28.51258245       0.0404      37.7549
       lambda2  29.45562567       0.0074     121.6742
            T2  29.95893332       0.0086     347.3450
            R2  30.04106668       0.0012     197.5592
            K2  30.08213725       0.0398       7.8449
# AVERAGE (Z0) =  29898.7480969
# SLOPE OF REMOVED LINEAR TREND =  0.0
```

Table 2: Harmonic Analysis Result for Seafloor Pressure Data Series 1.

```
(Canopy 32bit) Putris-MacBook-Pro:range1_n putriakmal$ ../tappy.py analysis
1200C_range1_n.txt data_def_sea.txt --linear_trend
#         NAME         SPEED             H         PHASE
#         ====         =====             =         =====
            Mm   0.54437433       0.0540     180.5368
           MSf   1.01589594       0.0419     359.8103
           2Q1  12.85428677       0.0440      37.8190
            Q1  13.39866110       0.2236     230.5941
            O1  13.94303543       1.1840      60.8366
           NO1  14.49669429       0.0190     266.6529
            K1  15.04106863       1.8285      78.5863
            J1  15.58544296       0.1048     282.6733
           OO1  16.13910182       0.0695     122.9530
          ups1  16.68347615       0.0093      19.4086
          MNS2  27.42383379       0.0109      72.9281
           mu2  27.96820812       0.0450     323.3611
            N2  28.43972973       0.3481     124.5469
            M2  28.98410406       1.2184     332.2025
            L2  29.52847839       0.0398     175.0034
            S2  30.00000000       0.1765     320.1305
          eta2  30.62651159       0.0113     126.7873
          2SM2  31.01589594       0.0039      69.1046
           MO3  42.92713949       0.0073     119.3502
            M3  43.47615609       0.0204     256.0752
           MK3  44.02517269       0.0011     279.9731
           SK3  45.04106863       0.0206      82.2331
           MN4  57.42383379       0.0082     104.3307
            M4  57.96820812       0.0217     330.2713
           SN4  58.43972973       0.0111     160.8127
           MS4  58.98410406       0.0270     348.3673
            S4  60.00000000       0.0102       1.4701
          2MN6  86.40793785       0.0072     344.6484
            M6  86.95231218       0.0129     175.8688
          2MS6  87.96820812       0.0020      92.7831
          2SM6  88.98410406       0.0051     245.6195
            S6  90.00000000       0.0109      97.4593
            M8 115.93641624       0.0093      49.5478
# INFERRED CONSTITUENTS
#         NAME         SPEED             H         PHASE
#         ====         =====             =         =====
          rho1  13.47151382       0.0450     209.2619
            M1  14.49205203       0.0841      59.2754
            P1  14.95893137       0.6052       7.4828
           2N2  27.89535540       0.0317      52.5943
           nu2  28.51258245       0.0463      39.2236
       lambda2  29.45562567       0.0085     120.2164
            T2  29.95893332       0.0104     164.3232
            R2  30.04106668       0.0014      14.2851
            K2  30.08213725       0.0480     184.4415
# AVERAGE (Z0) =  29746.9367138
# SLOPE OF REMOVED LINEAR TREND =  0.0
```

Table 3: Harmonic Analysis Result for Formation Pressure Data Series 2.

```
(Canopy 32bit) Putris-MacBook-Pro:range2B_rev putriakmal$ ../tappy.py
analysis 1200C_range2B_rev.txt data_def_fm.txt --linear_trend
#         NAME         SPEED             H         PHASE
#         ====         =====             =         =====
            Mm   0.54437433       0.0264     194.3783
           MSf   1.01589593       0.0268     356.7338
           2Q1  12.85428678       0.0376      40.1644
            Q1  13.39866111       0.2284     230.4904
            O1  13.94303544       1.0600      58.9391
           NO1  14.49669430       0.1437     248.7466
            K1  15.04106863       1.4553      73.0643
            J1  15.58544295       0.0909     283.6618
           OO1  16.13910181       0.0734     129.6333
          ups1  16.68347614       0.0113     317.5875
          MNS2  27.42383380       0.0068     175.7168
           mu2  27.96820813       0.0108     268.3322
            N2  28.43972974       0.2715     128.7221
            M2  28.98410407       1.0255     327.8799
            L2  29.52847839       0.0403     192.7598
            S2  30.00000000       0.1777     310.2001
          eta2  30.62651158       0.0054      80.5920
          2SM2  31.01589593       0.0043     225.9056
           MO3  42.92713950       0.0045     292.1393
            M3  43.47615610       0.0212     254.5496
           MK3  44.02517269       0.0055     248.6291
           SK3  45.04106863       0.0093      14.3246
           MN4  57.42383380       0.0029      12.0515
            M4  57.96820813       0.0190     209.8833
           SN4  58.43972974       0.0051      50.6367
           MS4  58.98410407       0.0123     252.9020
            S4  60.00000000       0.0056     131.3708
          2MN6  86.40793787       0.0036     284.2663
            M6  86.95231220       0.0073     132.2722
          2MS6  87.96820813       0.0049     147.2333
          2SM6  88.98410407       0.0030      81.1008
            S6  90.00000000       0.0038     289.0800
            M8 115.93641626       0.0001      18.1816
# INFERRED CONSTITUENTS
#         NAME         SPEED             H         PHASE
#         ====         =====             =         =====
          rho1  13.47151383       0.0403     358.0573
            M1  14.49205203       0.0753     274.1582
            P1  14.95893137       0.4817      99.3735
           2N2  27.89535541       0.0267     168.9810
           nu2  28.51258246       0.0390     214.0187
       lambda2  29.45562567       0.0072      84.5263
            T2  29.95893332       0.0105     317.5981
            R2  30.04106668       0.0014     102.7579
            K2  30.08213725       0.0483      60.0834
# AVERAGE (Z0) =  29915.8020328
# SLOPE OF REMOVED LINEAR TREND =  0.0
```

Table 4: Harmonic Analysis Result for Seafloor Pressure Data Series 2.

```
(Canopy 32bit) Putris-MacBook-Pro:range2B_rev putriakmal$ ../tappy.py
analysis 1200C_range2B_rev.txt data_def_sea.txt --linear_trend
#        NAME        SPEED            H        PHASE
#        ====        =====            =        =====
           Mm   0.54437433       0.0340     191.1551
          MSf   1.01589593       0.0282     349.3706
          2Q1  12.85428678       0.0456      41.9628
           Q1  13.39866111       0.2734     230.8198
           O1  13.94303544       1.2695      59.9540
          NO1  14.49669430       0.1688     250.0094
           K1  15.04106863       1.7453      73.7489
           J1  15.58544295       0.1076     283.9928
          OO1  16.13910181       0.0897     126.7392
         ups1  16.68347614       0.0111     315.0592
         MNS2  27.42383380       0.0103     173.4030
          mu2  27.96820813       0.0077     303.0057
           N2  28.43972974       0.3217     128.0771
           M2  28.98410407       1.1767     327.2987
           L2  29.52847839       0.0473     188.0677
           S2  30.00000000       0.2028     307.6331
         eta2  30.62651158       0.0060      63.3674
         2SM2  31.01589593       0.0010     247.7744
          MO3  42.92713950       0.0025       0.4577
           M3  43.47615610       0.0251     237.8178
          MK3  44.02517269       0.0106     125.6043
          SK3  45.04106863       0.0123      44.4608
          MN4  57.42383380       0.0045     179.4187
           M4  57.96820813       0.0099      10.6904
          SN4  58.43972974       0.0031     110.1378
          MS4  58.98410407       0.0205     354.3658
           S4  60.00000000       0.0056      54.0799
         2MN6  86.40793787       0.0035     263.5507
           M6  86.95231220       0.0072     150.9800
         2MS6  87.96820813       0.0018     237.0296
         2SM6  88.98410407       0.0012      60.1511
           S6  90.00000000       0.0049     277.9869
           M8 115.93641626       0.0026     118.1611
# INFERRED CONSTITUENTS
#        NAME        SPEED            H        PHASE
#        ====        =====            =        =====
         rho1  13.47151383       0.0482     358.0775
           M1  14.49205203       0.0901     274.1731
           P1  14.95893137       0.5777      99.3859
          2N2  27.89535541       0.0306     169.0080
          nu2  28.51258246       0.0447     214.0246
      lambda2  29.45562567       0.0082      84.5001
           T2  29.95893332       0.0120     317.5547
           R2  30.04106668       0.0016     102.7117
           K2  30.08213725       0.0552      60.0358
# AVERAGE (Z0) =  29746.8829899
# SLOPE OF REMOVED LINEAR TREND =  0.0
```

Table 5: Harmonic Analysis Result for Formation Pressure Data Series 3.

```
Putris-MacBook-Pro:range3B putriakmal$ ../tappy.py analysis 1200C_range3B_press.txt data_def_fm.txt
--linear_trend
#        NAME        SPEED            H        PHASE
#        ====        =====            =        =====
          Ssa   0.08213725       0.0556      80.1546
          MSm   0.47152161       0.0108      38.5801
           Mm   0.54437433       0.0401     258.1849
          MSf   1.01589594       0.0255     257.6236
           Mf   1.09803319       0.1153       9.0296
          2Q1  12.85428678       0.0309      48.4810
         nuJ1  12.92713950       0.0394      93.6537
           Q1  13.39866111       0.2280     230.5022
         rho1  13.47151383       0.0376     280.1048
           O1  13.94303544       1.1464      61.0679
          MP1  14.02517269       0.0260     136.3257
          NO1  14.49669430       0.1292     218.0346
         chi1  14.56954702       0.0195     307.3894
           P1  14.95893137       0.4538      57.6050
           K1  15.04106863       1.5985      74.9700
         phi1  15.12320588       0.0222      21.3139
       theta1  15.51259023       0.0177     223.6466
           J1  15.58544296       0.0867     279.0763
          SO1  16.05696456       0.0156     137.4788
          OO1  16.13910182       0.0968     130.8856
         ups1  16.68347615       0.0146     351.0615
         MNS2  27.42383379       0.0050     166.6512
          2N2  27.89535540       0.0281     281.7093
          mu2  27.96820812       0.0063     328.6353
           N2  28.43972973       0.2564     123.0887
          nu2  28.51258245       0.0537     172.2125
           M2  28.98410406       1.0029     326.6951
         MKS2  29.06624132       0.0052     261.1310
      lambda2  29.45562567       0.0169     149.8679
           L2  29.52847839       0.0313     178.8356
           S2  30.00000000       0.1584     310.3549
           K2  30.08213725       0.0293     314.7388
         MSN2  30.54437433       0.0068      30.5647
         eta2  30.62651158       0.0062      91.4376
         2SM2  31.01589594       0.0056     269.9433
          MO3  42.92713950       0.0085     277.1721
           M3  43.47615609       0.0196     242.0198
          SO3  43.94303544       0.0081     227.2015
          MK3  44.02517269       0.0061     246.3294
          SK3  45.04106863       0.0077       2.9615
          MN4  57.42383379       0.0030     354.4066
           M4  57.96820812       0.0164     210.0919
          SN4  58.43972973       0.0011     337.9813
          MS4  58.98410406       0.0103     281.3336
          MK4  59.06624132       0.0061     297.3330
           S4  60.00000000       0.0035     219.9778
         2MN6  86.40793786       0.0040     262.8450
           M6  86.95231219       0.0060     126.2008
         2MS6  87.96820812       0.0019     168.6256
         2SM6  88.98410406       0.0001     199.4752
           S6  90.00000000       0.0003     353.0380
           M8 115.93641625       0.0009       8.8196

# INFERRED CONSTITUENTS
#        NAME        SPEED            H        PHASE
#        ====        =====             =       =====
           M1  14.49205203       0.0814       2.8926
           T2  29.95893332       0.0093       8.0743
           R2  30.04106668       0.0013     176.4759
# AVERAGE (Z0) =  29921.0511145
# SLOPE OF REMOVED LINEAR TREND =  0.0
```

Table 6: Harmonic Analysis Result for Seafloor Pressure Data Series 3.

```
Putris-MacBook-Pro:range3B putriakmal$ ../tappy.py analysis 1200C_range3B_press.txt
data_def_sea.txt --linear_trend

#        NAME        SPEED            H        PHASE
#        ====        =====            =        =====
          Ssa   0.08213725       0.0320     282.4636
          MSm   0.47152161       0.0208      17.8542
           Mm   0.54437433       0.0520     258.2491
          MSf   1.01589594       0.0248     257.1827
           Mf   1.09803319       0.1252       8.7435
          2Q1  12.85428678       0.0380      54.5514
         nuJ1  12.92713950       0.0464      99.2681
           Q1  13.39866111       0.2722     230.8040
         rho1  13.47151383       0.0451     279.7261
           O1  13.94303544       1.3842      61.9843
          MP1  14.02517269       0.0350     121.9490
          NO1  14.49669430       0.1434     300.4224
         chi1  14.56954702       0.0227     307.6155
           P1  14.95893137       0.5410      58.0067
           K1  15.04106863       1.9173      75.9863
         phi1  15.12320588       0.0242      47.1439
       theta1  15.51259023       0.0184     226.7833
           J1  15.58544296       0.1017     280.6070
          SO1  16.05696456       0.0199     122.6193
          OO1  16.13910182       0.1144     132.1947
         ups1  16.68347615       0.0192     333.9490
         MNS2  27.42383379       0.0046     148.5229
          2N2  27.89535540       0.0333     283.6133
          mu2  27.96820812       0.0160       8.9513
           N2  28.43972973       0.2922     121.6259
          nu2  28.51258245       0.0588     178.8229
           M2  28.98410406       1.1561     324.7062
        MKS2  29.06624132       0.0206     221.9041
      lambda2  29.45562567       0.0193     121.9898
           L2  29.52847839       0.0367     161.7920
           S2  30.00000000       0.1907     304.7934
           K2  30.08213725       0.0457     299.5723
         MSN2  30.54437433       0.0118      15.2557
         eta2  30.62651158       0.0074      51.9386
         2SM2  31.01589594       0.0024     341.0761
          MO3  42.92713950       0.0036     224.1695
           M3  43.47615609       0.0273     229.8328
          SO3  43.94303544       0.0064      57.4656
          MK3  44.02517269       0.0093     107.2915
          SK3  45.04106863       0.0109      31.2389
          MN4  57.42383379       0.0128     219.2956
           M4  57.96820812       0.0258      75.4035
          SN4  58.43972973       0.0042     315.4136
          MS4  58.98410406       0.0259      48.7648
          MK4  59.06624132       0.0047     140.3732
           S4  60.00000000       0.0044     117.4053
         2MN6  86.40793786       0.0054     253.6613
           M6  86.95231219       0.0086     122.0207
         2MS6  87.96820812       0.0064     104.1290
         2SM6  88.98410406       0.0033      98.7068
           S6  90.00000000       0.0014      39.3191
           M8 115.93641625       0.0001     183.1228
# INFERRED CONSTITUENTS
#        NAME        SPEED            H        PHASE
#        ====        =====          =        =====
           M1  14.49205203       0.0983       6.0511
           T2  29.95893332       0.0112       7.9798
           R2  30.04106668       0.0015     176.3763
# AVERAGE (Z0) =  29747.0454099
# SLOPE OF REMOVED LINEAR TREND =  0.0
```

Table 7 : List of all body wave magnitude ≥ 5 occurred during the length of the CORK deployment in Borehole 1200C. (Data from the International Seismological Centre, 2011 and summarized by Vinas, 2013).

DATE	TIME	LAT	LON	DEPTH	AUTHOR	TYPE	MAG
3/29/01	2:01:24	12.636	143.643	33.7	NEIC	mb	5
4/2/01	6:50:04	11.845	147.385	33	HRVD	Mw	5.5
4/14/01	19:16:14	12.863	144.609	30.7	HRVD	Mw	5.3
4/27/01	18:58:46	15.727	147.442	35.2	HRVD	Mw	5.3
6/4/01	22:41:05	17.015	145.999	107.3	HRVD	Mw	5.7
8/3/01	22:13:01	11.802	142.717	21.8	NEIC	mb	5
8/4/01	18:55:10	15.757	147.404	50.1	HRVD	Mw	5.1
8/11/01	5:26:02	13.475	145.97	50	ISC	mb	5
10/11/01	21:06:55	11.97	142.17	54.2	NEIC	mb	5.1
10/12/01	15:02:20	12.716	144.975	61.8	HRVD	Mw	7
10/14/01	5:02:57	12.347	143.429	33	HRVD	Mw	5.2
10/23/01	12:04:53	14.197	145.223	97.1	NEIC	mb	5.1
10/31/01	19:12:13	14.797	147.014	24.8	MOS	mb	5
11/4/01	8:33:40	15.392	146.749	40.6	BJI	mb	5
11/22/01	11:18:33	11.913	142.671	33	MOS	mb	5
1/31/02	10:05:04	15.594	146.242	62.2	BJI	mb	5.1
2/9/02	18:27:01	13.749	144.622	155.1	BJI	mb	5.2
2/12/02	15:39:56	13.905	144.861	134.8	HRVD	Mw	5.8
3/3/02	11:52:32	13.015	143.695	140.1	BJI	mb	5.1
3/23/02	3:06:16	11.983	142.907	17.2	HRVD	Mw	5.2
4/10/02	11:47:23	11.515	142.068	36.7	ISC	MS	5
4/14/02	5:58:34	14.466	144.282	411.8	BJI	mb	5.1
4/15/02	3:52:07	13.011	143.823	121.2	HRVD	Mw	5.4
4/26/02	16:06:05	13.032	144.688	69.1	HRVD	Mw	7
5/21/02	23:45:34	13.998	145.04	131.4	HRVD	Mw	5.2
7/19/02	3:37:54	12.185	143.323	47.4	HRVD	Mw	5.1
8/2/02	6:32:45	16.829	146.359	64	HRVD	Mw	5
8/11/02	0:59:13	13.159	145.448	62.2	BJI	mb	5
8/14/02	13:57:55	14.036	146.278	54.5	HRVD	Mw	6.5
9/4/02	19:40:38	13.198	144.748	53.7	BJI	mb	5
9/22/02	16:33:55	12.795	145.216	43.4	MOS	mb	5.1
11/5/02	1:32:01	11.7137	142.0969	44.2	MOS	mb	5.1
11/12/02	7:12:40	13.5941	145.0543	128.8	HRVD	Mw	5.3
12/8/02	8:16:50	12.3545	144.2381	34.7	HRVD	Mw	5.1
12/8/02	11:29:09	12.4297	144.3798	33	BJI	MS	5.4
12/8/02	14:47:40	12.3666	144.6107	57.7	MOS	mb	5.1